NASA TECHNICAL NOTE

NASA TN D-4445

NASA TN D-4445

NONCAVITATING PERFORMANCE OF TWO LOW-AREA-RATIO WATER JET PUMPS HAVING THROAT LENGTHS OF 7.25 DIAMETERS

by Nelson L. Sanger

Lewis Research Center
Cleveland, Ohio

NATIONAL AERONAUTICS AND SPACE ADMINISTRATION • WASHINGTON, D. C. • MARCH 1968

NASA TN D-4445

NONCAVITATING PERFORMANCE OF TWO LOW-AREA-RATIO WATER JET PUMPS HAVING THROAT LENGTHS OF 7.25 DIAMETERS

By Nelson L. Sanger

Lewis Research Center
Cleveland, Ohio

NATIONAL AERONAUTICS AND SPACE ADMINISTRATION

For sale by the Clearinghouse for Federal Scientific and Technical Information
Springfield, Virginia 22151 – CFSTI price $3.00

CONTENTS

NONCAVITATING PERFORMANCE OF TWO LOW-AREA-RATIO WATER JET PUMPS HAVING THROAT LENGTHS OF 7.25 DIAMETERS

by Nelson L. Sanger

Lewis Research Center

SUMMARY

The performance of two jet pumps having low nozzle- to throat-area ratios was evaluated in a water facility and compared to theoretically predicted performance. The purposes of the investigation were to gain a better insight into the flow mechanisms involved in low-area-ratio jet pumps, and to compare the abilities of two existing one-dimensional analyses to predict jet pump performance over a wide range of operating conditions.

Two nozzles were evaluated experimentally and the test pump consisted of one of the two nozzles and one test section, the latter having a throat diameter of 1.35 inches (3.43 cm), a throat length of 7.25 diameters, and a diffuser included angle of $8^{\circ}6'$ (0.141 rad). The nozzles had exit diameters corresponding to nozzle- to throat-area ratios of 0.066 and 0.197. Each nozzle was operated at several spacings of the nozzle exit upstream from the throat entrance over a range of from 0 to 3 throat diameters.

For an area ratio of 0.066, a maximum measured efficiency of 29.5 percent was achieved at a fully inserted nozzle position (nozzle exit plane coinciding with throat entrance plane); for an area ratio of 0.197, a maximum measured efficiency of 35.7 percent was achieved, also at a fully inserted nozzle position. Performance at maximum efficiency levels was maintained for both area-ratio jet pumps over a range of nozzle spacings from 0 to 1 throat diameter.

At small nozzle spacings (up to 1 throat diameter) a simple one-dimensional analysis predicted performance quite closely. The theory also demonstrated that low efficiencies exhibited at low ratios of secondary to primary (high pressure) flows are due to inefficient mixing, whereas low efficiencies at high flow ratios are due largely to friction losses. A modified theory, which attempted to account for the effect of the mixing profile in the throat, required more computational effort and did not improve correlation with experimental performance.

INTRODUCTION

One method being considered for generating relatively large quantities of power for applications in space vehicles is the use of a Rankine cycle system utilizing liquid metal as the working fluid (ref. 1). The jet pump has been utilized in the development of these space-oriented systems (refs. 2 to 4) because of its simplicity and inherent reliability; furthermore, it requires only a modest net positive suction head for cavitation-free operation and it can be installed in locations remote from mechanical power sources. A jet pump may have several applications in these systems. It may be used as an inducer stage for the boiler feed pump, a recirculating boiler pump, or as an auxiliary lubrication or cooling pump. The probable source of the high-pressure driving (primary) fluid for such jet pump applications will be from mechanical or electromagnetic pumps. In order to keep size, weight, and power requirements of the main pumps low, it will be necessary to keep the amount of fluid recirculated (primary fluid) to the jet pump low. As a consequence, jet pumps which operate at high ratios of secondary to primary flowrates are required, and they are specified geometrically by low (< 0.25) ratios of the primary-nozzle-flow area to mixing-chamber (throat) area. There has been little commercial development of low-area-ratio jet pumps because they characteristically produce relatively low head rises.

Jet pumps are currently developed from a design procedure which does not completely specify geometry. The procedure is based on an analysis introduced in 1870 by J. M. Rankine (ref. 5) and presented in some detail in references 6 and 7. Although modifications to the one-dimensional analysis have been introduced (refs. 8 and 9), and the case of confined jet mixing studied extensively in recent years (refs. 10 to 12), the optimization of jet pump design is still dependent, to a large extent, on experimental testing and empirical procedures.

Even so, experimental determination of optimum geometrical configurations is a more formidable task than might be imagined for two principal reasons. The first reason is the large number of geometrical variables concerned: nozzle- to throat-area ratio, secondary inlet shape, nozzle exterior contour shape, primary nozzle-exit to throat-entrance spacing, throat length, and diffuser angle and length. The second reason is the interrelation of many of these variables - for example, nozzle spacing, throat length, and nozzle- to throat-area ratio all affect mixing characteristics in some manner. It is not surprising therefore that results from previous studies have not yielded consistent design recommendations; for example, recommended throat lengths (expressed in throat diameters) ranged from 3.5 to as much as 8.0 (refs. 6, 8, 13, and 14).

Although a relatively large amount of literature on jet pumps exists (refs. 3 to 9 and 13 to 16), few investigations deal with the basic flow processes involved. As a consequence, recommended design criteria may often vary considerably, as in the case of

throat length mentioned previously. It is therefore necessary to explore in more detail the basic fluid mechanics of jet pumps in order to produce more consistent designs.

In accordance with this, the object of the present investigation was twofold. First, it was desired to obtain a better insight into the flow mechanisms involved in jet pumps, particularly for low-area-ratio configurations. Nozzle spacing upstream from the throat entrance was selected as the prime geometric variable to be investigated in a jet pump having a relatively long throat. A long throat was chosen to permit mixing to be completed in the throat, thereby allowing mixing characteristics to be studied. The second objective of the investigation was to compare the ability of two analyses to predict jet pump performance over a wide range of operating conditions. The two analyses considered were the conventional one-dimensional analysis (refs. 5 to 7) and a modified one-dimensional analysis (refs. 8 and 9).

The experimental investigation was conducted using room-temperature tap water in a highly instrumented transparent plastic test section of circular cross section having a throat diameter of 1.35 inches (3.43 cm), a throat length of 9.78 inches (24.8 cm), and a diffuser with an included angle of $8^{\circ}6'$ (0.141 rad). Two separate nozzles, which provided area ratios of 0.066 and 0.197, were tested. Operating conditions included primary flow rates of from 28 to 83 gallons per minute (1.77×10^{-3} to 5.24×10^{-3} m^3/sec); secondary flow rates of 30 to 200 gallons per minute (1.89×10^{-3} to 2.62×10^{-3} m^3/sec) and primary nozzle inlet pressures of 35 to 110 psia (2.41×10^5 to 7.56×10^5 N/m^2 abs).

PERFORMANCE PREDICTION

PRINCIPLE OF OPERATION

The principle of operation of a jet pump is the transfer of energy and momentum from primary to secondary fluid through a process of turbulent mixing. A schematic representation of a jet pump is shown in figure 1, and the nomenclature is presented in appendix A. The primary fluid is pressurized by an independent source and is accelerated to high velocity in the nozzle. The secondary fluid is entrained by and mixed with the primary fluid in the constant diameter throat section. The mixed fluids then pass through the diffuser in which a portion of the velocity head is converted to static pressure.

The fundamental mechanism of jet pump operation is the turbulent mixing process, a complex process that is still not well understood. A schematic representation of the mixing velocity profile development in the throat is shown in figure 2. At the nozzle exit, the primary stream is essentially a core of constant high velocity fluid which is separated from the secondary stream by a region of high shear. Initially, the high shear region is made

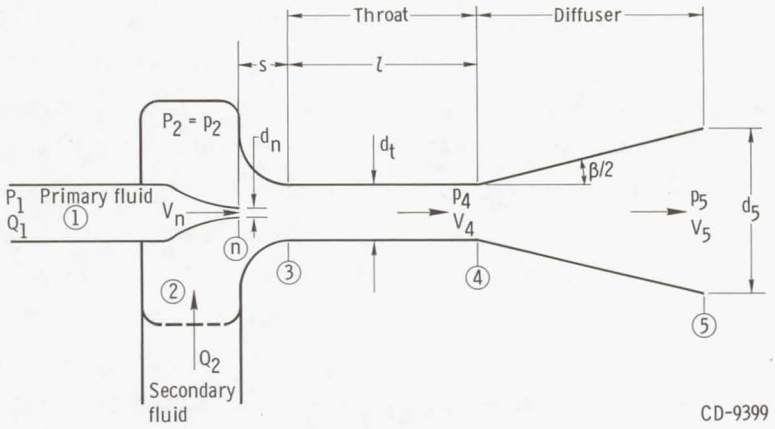

Figure 1. - Schematic representation of a jet pump.

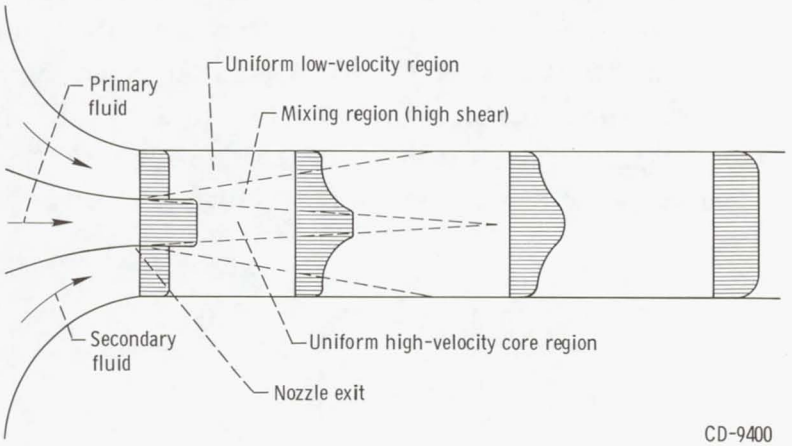

Figure 2. - Schematic representation of mixing velocity profile in throat of jet pump.

up of a thin sheet of vortices or eddies which give rise to mixing on the periphery of the high velocity core.

As axial distance from the nozzle exit is increased, the shear or mixing layer increases in thickness. The potential core region progressively grows smaller as its energy is dissipated to turbulence in the mixing layer. Due to the transport of momentum, the primary stream is decelerated while the secondary stream is accelerated. The lateral growth of the mixing layer continues until it finally meets the jet centerline and the constant velocity core disappears. Eventually, the mean velocity profile across the duct assumes an equilibrium shape (ref. 11).

Considerable effort has been devoted to the study of the mixing characteristics of free jets (ref. 17), but until recently relatively little effort has been devoted to the prob-

lem of confined or ducted jets, which is the case of interest in jet pump flow. The bounding walls in confined jet flow cause the formation of a pressure gradient which, combined with wall friction losses, considerably complicates the mathematical analysis. Furthermore, in a jet pump, mixing can occur in nonconstant diameter sections such as the converging inlet section between the primary nozzle exit plane and the throat entrance, and in the diffuser immediately downstream of the throat exit. Although progress is being made in the study of confined jet mixing, there is presently no easily applied procedure which can be used to specify optimum nozzle position, throat length, and diffuser configuration for a jet pump of given area ratio.

ANALYSIS

Jet pump performance may be predicted by either of two methods available in the literature. Although both are based on the same fundamental assumptions, one contains some additional refinement terms and is more complex to apply. This analysis is referred to herein as the modified analysis. The conventional analysis is compared, in this report, to the modified analysis to determine which of the two is more useful in the design of jet pumps. The performance parameters used in these analyses are described first.

Performance Parameters

The four fundamental parameters of jet pump analysis and design are presented in nondimensional form in accord with the conventions of the jet pump literature. These parameters are nozzle- to throat-area ratio, $R = A_n/A_t$, secondary- to primary-flow ratio $M = Q_2/Q_1$, and head ratio, $N = (H_5 - H_2)/(H_1 - H_5)$ (fig. 1). Efficiency is conveniently expressed as $\eta = MN$, the equivalent of net output power divided by net input power.

Conventional and Modified Analyses

The basic assumptions of both analyses presented herein are (1) both fluids are incompressible and of equal density, (2) nozzle spacing from throat entrance is zero, (3) nozzle wall thickness is zero, and (4) mixing is complete at throat exit. Assumptions (2) and (4) make it clear that this analysis cannot be used to optimize geometrical components. Determination, by experimental testing, of optimum throat length, nozzle spacing, diffuser configuration, and secondary inlet configuration for selected area

ratios remains, at present, the only alternative.

The analysis is one-dimensional and consists of an application of continuity, momentum, and energy equations across the jet pump. Friction losses are taken into account through the use of friction loss coefficients K, which are based on dimensionless total pressure losses in individual components of the pump, such as the primary nozzle, throat, and diffuser. The friction loss coefficient for each component may be determined either by estimating the values on the basis of information in the literature (refs. 6 to 8) or by calibrating the individual components. The latter method was utilized in this report and is discussed in appendix B.

In the conventional analysis, friction loss in the throat is accounted for by a friction loss coefficient based on the assumption of fully developed turbulent pipe flow. This is clearly approximate. The mixing profile only becomes fully developed in shape near the end of the throat if the throat is of sufficient length. In the modified analysis, the expression for friction loss in the throat contains a term which attempts to take into account the development of the mixing profile. The modified analysis is discussed in references 8 and 9 and is also developed in appendix B. Both analyses result in formulas for N and η as functions of M, R, and the values of the various loss coefficients K.

The formulas for head ratio N resulting from both analyses are reproduced below for convenience. The formula for efficiency η is obtained by multiplying the expression for head ratio N by the flow ratio M.

Conventional analysis:

$$N = \frac{2R + \frac{2R^2M^2}{1 - R} - (1 + K_t + K_d)R^2(1 + M)^2 - (1 + K_s)\frac{R^2M^2}{(1 - R)^2}}{1 + K_p - 2R - \frac{2R^2M^2}{1 - R} + R^2(1 + M)^2(1 + K_t + K_d)} \tag{13}$$

Modified analysis:

$$N = \frac{2R + \frac{2R^2M^2}{1 - R} - R^2(1 + M)^2(1 + K_t' + K_t'' + K_d) - \frac{R^2M^2}{(1 - R)^2}(1 + K_s + K_t')}{1 + K_p - 2R - \frac{2R^2M^2}{1 - R} + R^2(1 + M)^2(1 + K_t' + K_t'' + K_d) + K_t'\frac{R^2M^2}{(1 - R)^2}} \tag{34}$$

Component Losses

The jet pump is a relatively inefficient pumping device. However, little theoretical analysis of the comparative sources and relations of losses has been reported, despite the obvious assets to a designer that such knowledge would provide. With the aid of the conventional analysis it is possible to separate the losses and develop expressions for losses due to mixing and losses due to friction in each of the components. In appendix B the expressions for mixing and friction losses are completely developed and nondimensionalized. The results are summarized as follows:

Mixing loss:

$$\varphi_m = 1 + R^2 (1 + M)^3 - 2R(1 + M) + \frac{M^3 R^2}{(1 - R)^2} - \frac{2M^2 R^2 (1 + M)}{(1 - R)} \tag{19}$$

Primary-nozzle friction loss:

$$\varphi_p = K_p \tag{20}$$

Secondary-inlet friction loss:

$$\varphi_s = K_s \frac{R^2 M^3}{(1 - R)^2} \tag{21}$$

Throat friction loss:

$$\varphi_t = K_t R^2 (1 + M)^3 \tag{22}$$

Diffuser friction loss:

$$\varphi_d = K_d R^2 (1 + M)^3 \tag{23}$$

Overall friction loss:

$$\varphi_f = \varphi_p + \varphi_s + \varphi_t + \varphi_d$$

$$= K_p + \frac{K_s R^2 M^3}{(1 - R)^2} + (K_t + K_d) R^2 (1 + M)^3 \tag{24}$$

Total loss:

$$\varphi_l = \varphi_f + \varphi_m$$

$$= 1 + K_p + (1 + K_t + K_d) R^2 (1+M)^3 - 2R(1 + M) + (1 + K_s) \frac{M^3 R^2}{(1 - R)^2} - \frac{2M^2 R^2 (1 + M)}{(1 - R)} \tag{25}$$

The variation of mixing, friction, and overall loss with area ratio and flow ratio can thus easily be studied.

Axial Static Pressure Distributions

A very useful research parameter for study of the axial variation of static pressure in constant diameter jet pumps is the pressure coefficient C_p:

$$C_p = \frac{p_x - p_2}{\left(\frac{\gamma V_n^2}{2g}\right)} \tag{26}$$

where p_2 is the secondary inlet static pressure and p_x is any other static pressure in the pump. The numerator represents the pressure rise above secondary inlet pressure at any axial location in the jet pump. The denominator is the velocity head of the primary fluid at nozzle exit. The use of this parameter therefore permits direct comparison of data taken at different primary flow rates (i.e., different $V_n^2/2g$) and different secondary inlet pressures.

For a given operating point the value of C_p at throat inlet may be subtracted from the value at throat outlet, producing a parameter $\Delta C_{p,t}$, the rise in C_p in the throat.

A theoretical expression for $\Delta C_{p,t}$ can be derived (see appendix B) from the conventional one-dimensional analysis. The result is

$$\Delta C_{p,t} = 2R + \frac{2M^2R^2}{1 - R} - (2 + K_t)R^2(1 + M)^2 \tag{28}$$

APPARATUS

TEST FACILITY

Research Pump Loop

The test facility utilized was a closed-loop, continuous-circulation water tunnel. The main flow path consisted of 6-inch stainless-steel piping. A schematic diagram of the facility is shown in figure 3, and a photograph showing the control panel and test section is shown in figure 4. The total liquid capacity was approximately 350 gallons (1.325 m^3). The working fluid was tap water, deaerated to an air content of less than 5 ppm by mass. A 300-gallon (1.135-m^3) galvanized iron supply tank ("main tank") served as source for both primary and secondary fluids. The pressurized primary fluid was supplied by a commercial 20-horsepower (1481.4 W) motor-driven centrifugal pump

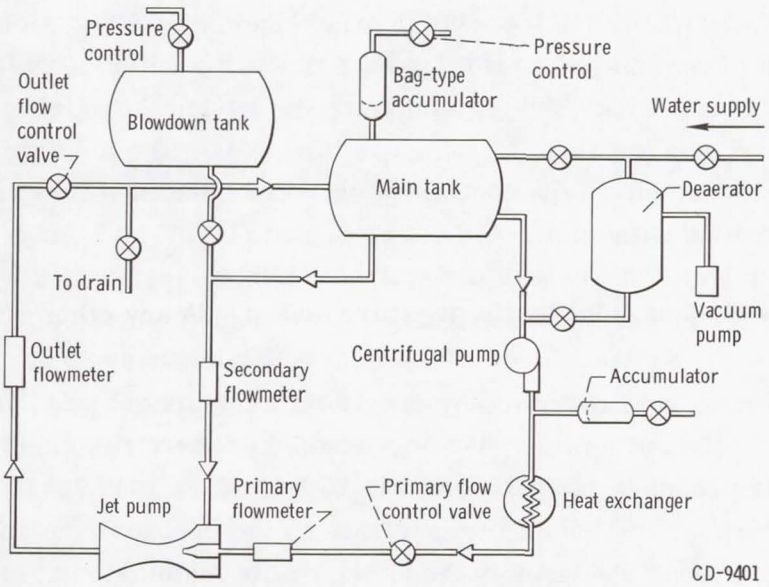

Figure 3. - Schematic of water jet pump test facility.

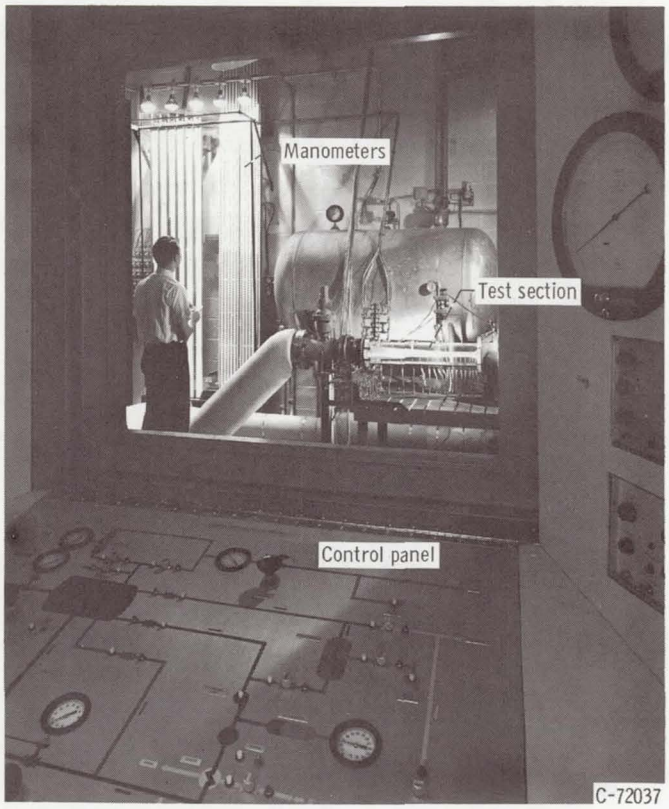

Figure 4. - Water jet pump test facility.

rated for a total head rise of 375 feet (114.3 m) of liquid at a 100-gallon-per-minute (6.31×10^{-3} m^3/sec) flow rate. The fluid passed through a filter capable of removing particles larger than 25 microns. Prior to entering the system, particles larger than 40 microns were removed by a separate filter. The flow rate of the primary fluid was varied by a pressure-balanced, plug-type control valve. The combined flow at the exit of the jet pump was controlled with an air-operated, 6-inch (15.25-cm) globe valve.

System water temperature was maintained within the range of 70° to 80° F (294° to 300° K) through the use of a shell and tube heat exchanger located in the primary stream.

System pressure was controlled by two 10-gallon bladder-type accumulators connected in parallel to the main tank. Air was used as pressurizing medium in the elastic bags; the operating pressure ranged from 4 to 25 psia (0.28 to 1.72×10^5 n/m^2 abs). Because of the accumulator method of pressurization, the pressurizing gas never contacted the system water, and air content was therefore easily maintained at a low level. One additional accumulator was used at the centrifugal pump outlet to dampen pump pulsations.

Auxiliary Systems

Two auxiliary systems were used: one controlled the air content of the water, and the other permitted dye injection and calibration test runs.

Deaeration system. - Subatmospheric pressures occurred in the inlet and throat sections of the jet pump under some operating conditions. Under these conditions air dissolved in the water is released from solution, and during the testing period is likely to collect in instrumentation lines. To avoid the errors associated with these conditions, a bypass deaeration system was incorporated into the test facility to reduce the air content of the test water.

Prior to testing, the water was circulated through a deaerator tank under high vacuum. When the air content was reduced to the desired level, the deaeration system was isolated and the test water was circulated in the main loop only. After a period of continuous testing, no significant increases in air content were measured. The air content was measured with a Van Slyke gas apparatus and expressed as parts per million by mass of air in water.

Blowdown system. - An alternate blowdown system (i.e. nonrecirculating) was provided to permit dye-injection mixing studies and test-section friction loss calibrations to be made. In this mode of operation an additional 300-gallon (1.135 m^3) tank ("blowdown tank" (fig. 3)) functioned as a supply tank for the secondary fluid, while the main tank supplied primary fluid only. Each tank was independently pressurized with air. Primary and secondary flows were supplied to the test section through the same piping as in closed-loop operation, and total flow was controlled by the same outlet control valve; but, after passing through the outlet valve, the flow was diverted to the drain. The main tank could also be isolated and flow from the blowdown tank used independently to calibrate the test sections for friction loss coefficients (K's).

TEST PUMP DESCRIPTION

The test pump (fig. 5) consisted of the following elements: the primary nozzle, the secondary fluid plenum, nozzle spacing shims, and the test section.

The stainless-steel plenum preceding the test section was $15\frac{1}{2}$ inches (39.35 cm) in diameter and had a capacity of about $4\frac{1}{2}$ gallons (1.70×10^{-2} m^3). Secondary fluid was supplied to it through two 3-inch (7.61 cm) outside-diameter pipes to provide a uniform radial distribution of flow. The test section was fabricated from acrylic plastic to enable visual observation and photographic studies to be made. Test facility piping arrangement fixed the overall test section length at 29.7 inches (75.4 cm).

	Static pressure taps																		Total pressure probes		
	Secondary inlet region		Throat									Diffuser									
Axial location from throat entrance, x/d_t	-0.9	-0.4	0.1	0.9	1.8	2.6	3.5	4.3	5.2	6.1	6.9	8.0	9.4	10.9	13.1	15.4	17.6	19.8	6.0	10.9	17.5

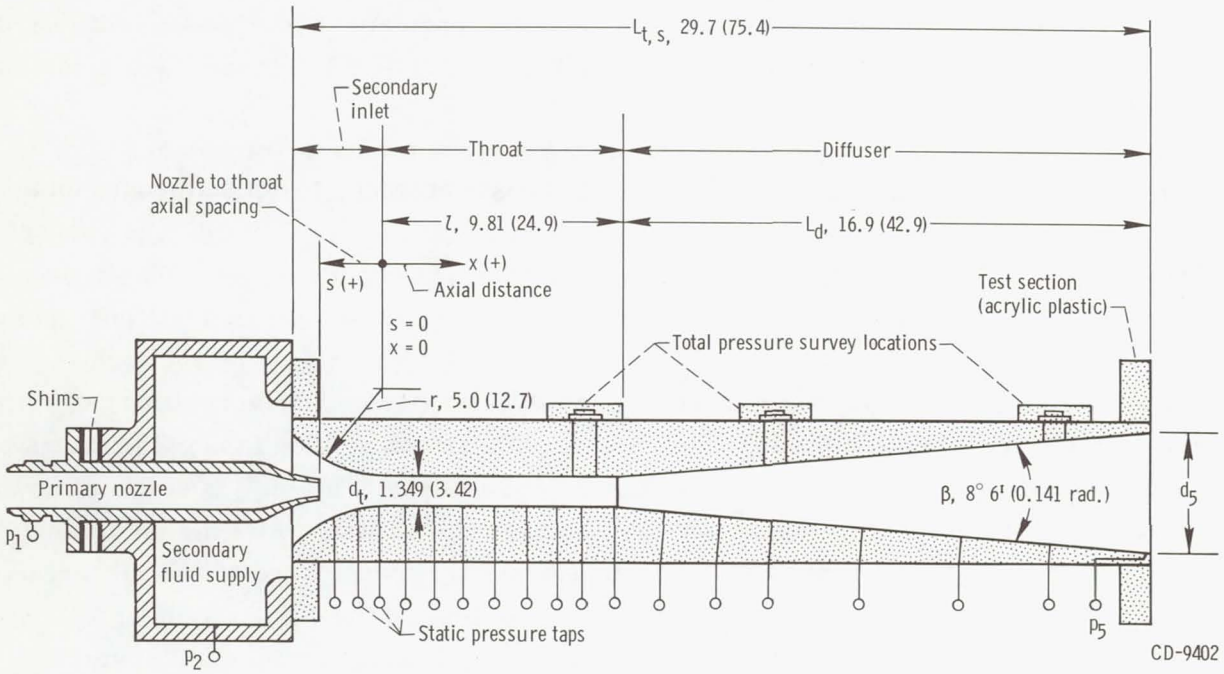

Figure 5. - Schematic diagram of test pump and location of static pressure taps and total pressure probes. Diameter ratio, $(d_5/d_t)^2$, 7.73. All dimensions are in inches (cm).

Previous investigations have established the superiority of a bell-mouth secondary inlet profile (refs. 8, 15, and 16). Therefore, a 5-inch (12.7-cm) circular-radius bell-mouth was used as inlet to a constant 1.35-inch-diameter (3.43-cm-diam) throat section.

Because optimum throat lengths reported in the literature ranged from 3.5 to 8 diameters the choice for throat length was flexible. One of the major objectives of the investigation was to study the mechanism of flow in low-area-ratio jet pumps. This could best be achieved by making the throat of sufficient length to allow mixing to be completed there. A throat length corresponding to 7.25 throat diameters, near the high end of the recommended range, was therefore selected.

Since diffuser performance is dependent on the shape of the inlet velocity profile, selection of a diffuser for jet pump application is related to the length of the throat, and to the extent that it influences mixing length requirements, to jet pump area ratio. When substantial mixing proceeds into the inlet of the diffuser there is a danger of separation, particularly in a jet pump where the low energy (secondary) fluid is located near the wall.

For jet pumps having throat lengths sufficient to provide an acceptable diffuser inlet velocity profile, a 6^{o} (0.105 rad) included angle is generally considered satisfactory. Whether it is smaller or greater than 6^{o} is determined largely by secondary effects such as jet pump area ratio, surface roughness, and mixing characteristics. References 6 and 8, for example, recommend included angles of 5.5^{o} and 5^{o} (0.096 and 0.087 rad), respectively. On the other hand, in reference 13 diffuser included angles of about 8^{o} (0.14 rad) and diffuser outlet- to inlet-area ratios no greater than 4 to 5 are recommended. Since the throat length in the present design was relatively long, the larger value of diffuser angle, $8^{o}6'$ (0.141 rad), was considered more applicable. Test facility size then determined the diffuser outlet- to inlet-area ratio to be 7.73.

Plugs were installed in the top of the test section at axial locations of 6.0, 10.9, and 17.5 throat diameters, measured from the throat entrance, to accommodate total pressure probes. The location of the first survey probe was in the throat near the entrance to the diffuser, and the other two were located in the diffuser (fig. 5). Static pressure taps of 0.020 inch (0.051 cm) in diameter were installed at 18 axial locations: 2 in the secondary inlet region, 9 in the throat, and 7 in the diffuser. The two taps in the secondary inlet region were drilled vertically (see fig. 5), and thus were inclined to the flow at angles of 15^{o} and 5^{o} (0.261 and 0.087 rad), respectively. The error introduced by such inclinations of static pressure orifices to the flow is discussed in reference 18 where no effective error was reported up to angles of inclination of 30^{o} (0.522 rad). Therefore, no corrections were applied to the static pressure data reported herein.

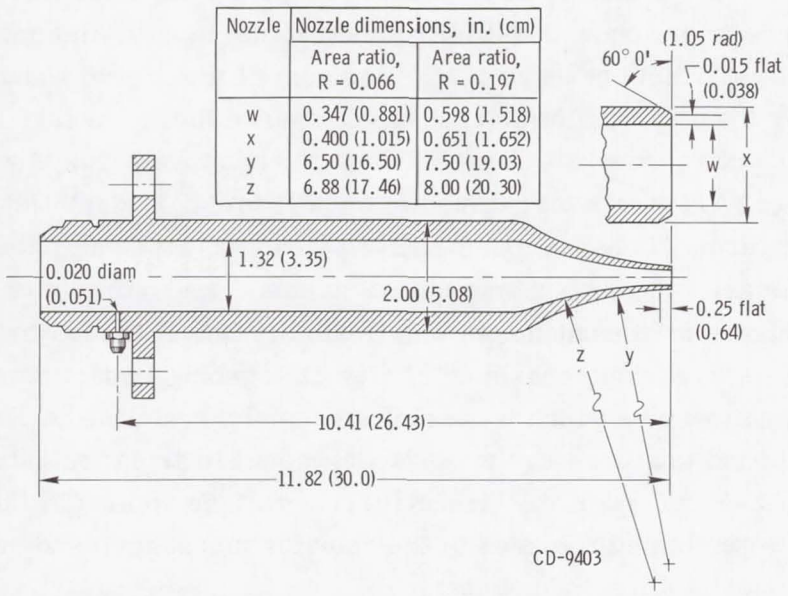

Figure 6. - Jet pump primary nozzles. (All dimensions are in inches (cm).)

Two stainless-steel primary nozzles were tested and the significant dimensions of each are indicated in figure 6. A large radius exterior nozzle contour was designed to prevent blockage by the nozzle shoulder of the secondary stream when the nozzle was operated in a fully inserted position. Each nozzle was equipped with an upstream static pressure tap 0.020 inch (0.051 cm) in diameter. The spacing of the nozzle exit from the throat entrance was provided by the use of shims inserted between the nozzle flange and a reference surface on the plenum.

INSTRUMENTATION

The 18 test-section static pressures and the secondary inlet pressure in the plenum were measured by banks of 120-inch (3.05-m) mercury manometers. The overall jet pump static pressure rise was also read directly on the U-tube manometers, one using mercury for high-pressure rises and the other using X-DI-Bromcethylene (specific gravity = 1.75 at 55° F, 286° K) as an indicating fluid for low-pressure rises. All banks of manometers were photographed for data reduction purposes. Nozzle-inlet static pressure was measured by a 12-inch (30.5-cm) Bourdon tube gage (0-200 psia scale, 0 to 13.98×10^5 N/m^3 abs), accurate to within ±0.2 psi (0.014 N/m^2).

The flow rates of the primary and secondary fluids were measured by turbine flowmeters with output registered on frequency counters. The flow rate of the mixed fluid ("total flow") was measured by a Venturi flowmeter located between the jet pump outlet and the outlet flow control valve. The Venturi pressure difference was read on a pair of U-tube manometers (mercury and X-DI-Bromoethylene) in a similar manner as described previously for the jet pump pressure rise. The sum of the primary and secondary flow rates recorded by the turbine flowmeters was compared to the Venturi-measured total flow rate over the entire flow rate range. The agreement was always within ±2 percent.

Temperature, which was maintained in the 70° to 80° F (294° to 300° K) range, was monitored at several locations. Closed-ball-type copper-constantan thermocouples were located in the primary, secondary, and mixed streams, and output was recorded on a strip chart potentiometer recorder.

The total pressure probe consisted of a single opening impact tube mounted in the leading edge of a hollow tube which was reinforced and streamlined. Pressure from the probe was transmitted to a pressure transducer whose electrical output was recorded on the X-scale of an X-Y recorder. A direct-current voltage applied to the probe actuator was divided by a potentiometer geared to the actuator mechanism and recorded as radial position on the Y-scale of the X-Y plotter.

Dye mixing patterns were photographed with a 70-millimeter still camera coupled to a flash unit.

The estimated errors (instrument and readability combined) of the principal measured variables are as follows:

Head rise and static pressure (manometers), percent	$< \pm 0.7$
Inlet pressure (primary stream), percent	$< \pm 0.6$
Flow rate (primary stream), percent	$< \pm 1.0$
Flow rate (secondary stream), percent	$< \pm 2.0$
Temperatures, deg F (K)	$< \pm 2.0$ (1.1)
Total pressure surveys	
Total pressure, percent	$< \pm 2.0$
Radial position, percent	$< \pm 5.0$

EXPERIMENTAL PROCEDURE

For the test section under consideration, jet pump noncavitating performance was obtained using the two nozzles represented in figure 6. Their exit diameters corresponded to area ratios of R = 0.066 and 0.197.

TESTS OF SMALLER AREA RATIO JET PUMP, R = 0.066

Noncavitating performance tests using the nozzle having an exit diameter of 0.347 inch (0.88 cm) were run for a range of nozzle spacings from throat inlet of 0 to 3.04 throat diameters. Primary flow rate was fixed at 28 gallons per minute (1.77×10^{-3} m^3/sec) and secondary inlet pressure at 15 psia (1.03×10^5 N/m^2 abs). For each nozzle position, performance evaluations were conducted over a range of secondary flows corresponding to values of flow ratio M from 1.15 to a maximum of 5.39. For nozzle spacings of 0, 1.54, and 3.04 and a secondary inlet pressure of 15 psia (1.03×10^5 N/m^2 abs). experimental performance was also recorded at a primary flow rate of 35 gallons per minute (2.21×10^{-3} m^3/sec) over a range in flow ratio M from 0.90 to a maximum of 5.30. No significant effects of primary flow rate on overall performance were observed.

Total pressure surveys were conducted at three nozzle positions as follows. The nozzle spacing for which best efficiency resulted ($s/d_t = 0$) was selected; the spacing beyond which efficiency began to deteriorate ($s/d_t = 1.05$) was also selected; and finally, a high spacing well into the low efficiency range ($s/d_t = 2.58$) was selected. For each nozzle spacing, surveys were taken at the flow ratio which corresponded to peak efficiency for that spacing, and at M = 2.5 and 5.0. Two sets of surveys were taken, one at a primary flow rate of 28 gallons per minute (1.77×10^{-3} m^3/sec) and the other at

35 gallons per minute (2.21×10^{-3} m^3/sec). A comparison yielded no evidence of an effect of primary flow rate on mixing characteristics.

For the blowdown mode of operation, dye (nigrosene black) was injected into the primary fluid and the resultant mixing pattern was photographed. The tests were conducted at two different primary flow rates (Q_1 = 25 and 31 gal/min, 1.58 and 1.96×10^{-3} m^3/sec) for nozzle spacings of 0 and 1.55 throat diameters.

TESTS OF LARGER AREA RATIO JET PUMP, R = 0.197

Noncavitating performance tests using the nozzle having an exit diameter of 0.598 inch (1.52 cm) were run for a range of nozzle spacings from throat inlet of 0 to 3.02 throat diameters. Primary flow rate was fixed at 63 gallons per minute (3.98×10^{-3} m^3/sec) and secondary inlet pressure of 15 psia (1.03×10^5 N/m^2 abs). For each nozzle position performance evaluations were conducted over a range of secondary flows corresponding to values of flow ratio M from 0.41 to a maximum of 2.50.

Total pressure surveys were conducted at three nozzle spacing positions. Identical criteria were applied for the selection of nozzle spacing positions as were used for the R = 0.066 surveys. The nozzle spacings selected were s/d_t = 0, 0.96, and 2.68. Primary flow rate was held constant at Q_1 = 63 gallons per minute (3.98×10^{-3} m^3/sec). For each nozzle position, surveys were taken at the flow ratio which corresponded to peak efficiency for that position and at M = 0.91 and 2.1.

RESULTS AND DISCUSSION

EXPERIMENTAL RESULTS

Overall Performance

Performance curves for the 0.066 and 0.197 area ratio jet pumps are presented in figures 7(a) and (b), respectively. Data presented for seven different nozzle spacings for the R = 0.066 pump and six nozzle spacings for the R = 0.197 pump are plotted as efficiency η and head ratio N against flow ratio M. A peak measured efficiency of 29.5 percent for the R = 0.066 pump was achieved at a fully inserted nozzle position ($s/d_t = 0$) and at a flow ratio of M = 3.5 (fig. 7(a-1)). The head ratio N corresponding to this flow ratio and nozzle position was N = 0.084 (fig. 7(a-2)). The R = 0.197 pump achieved a peak measured efficiency of 35.7 percent also at a fully inserted nozzle posi-

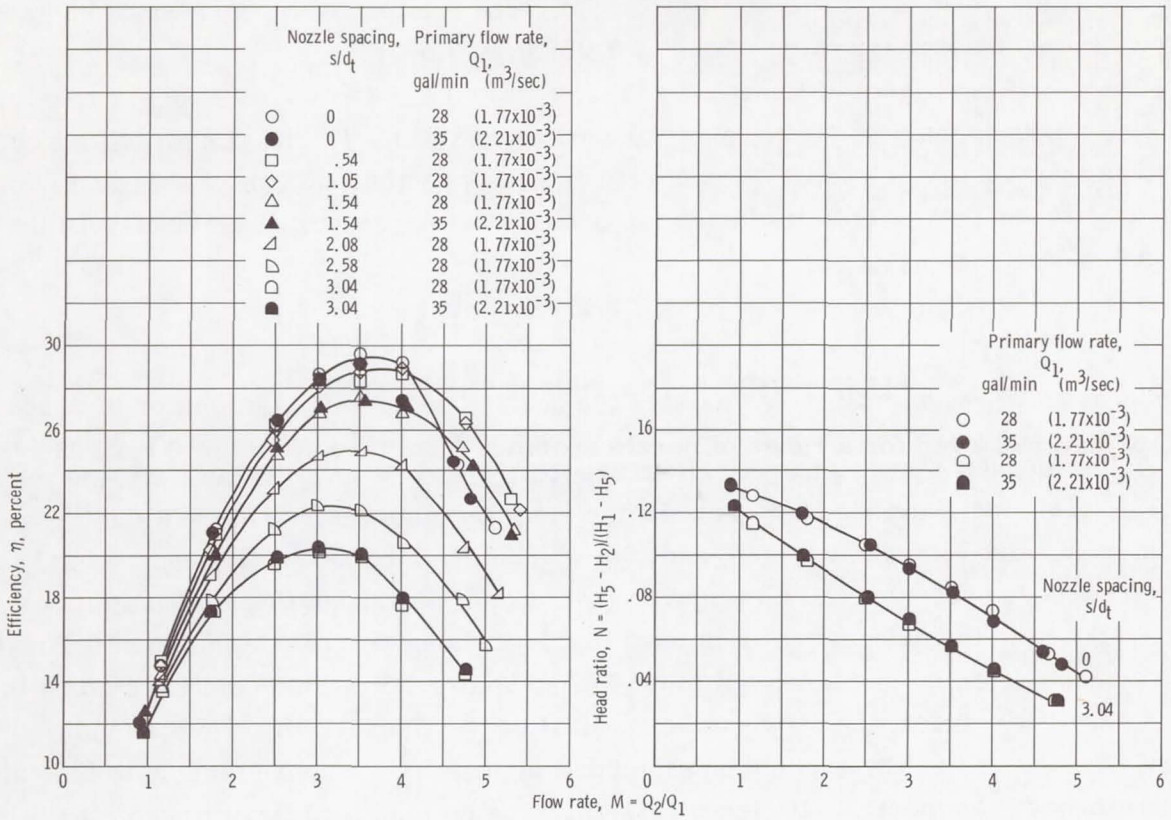

(a-1) Efficiency.

(a-2) Head ratio.

(a) Area ratio, R = 0.066.

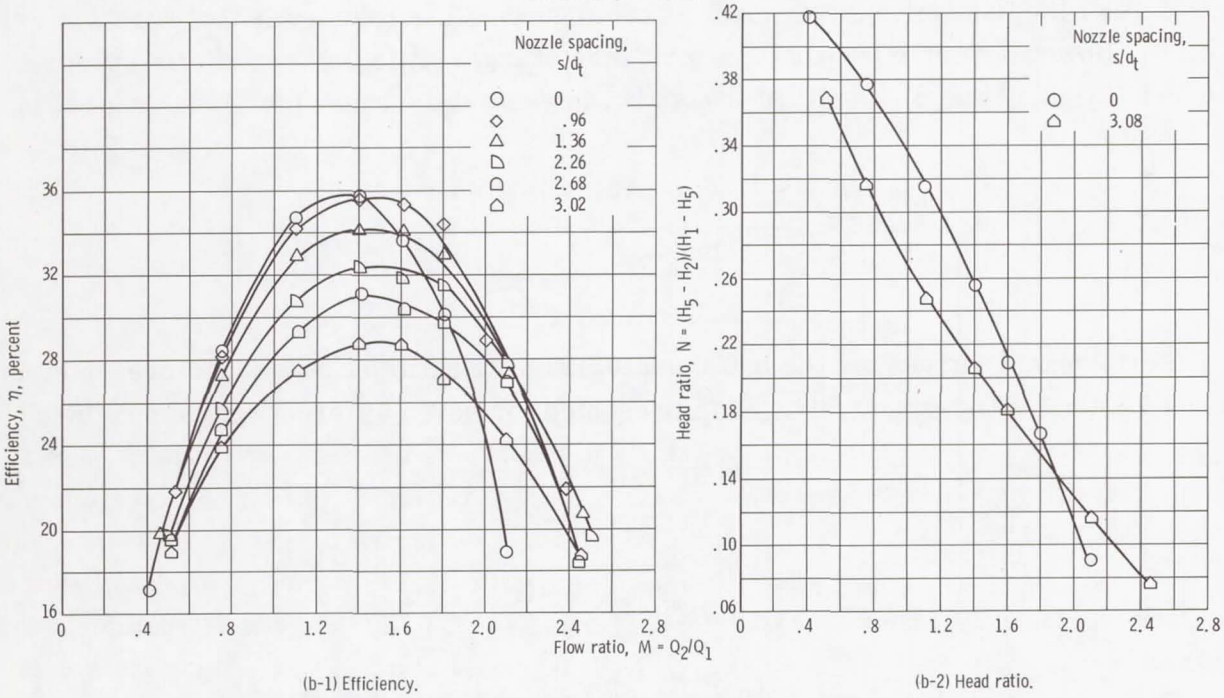

(b-1) Efficiency.

(b-2) Head ratio.

(b) Area ratio, R = 0.197. Primary flow rate, 63 gallons per minute (3.97×10^{-3} m^3/sec).

Figure 7. - Noncavitating performance of jet pumps.

tion and at a flow ratio of $M = 1.40$ (fig. 7(b-1)). The head ratio N corresponding to this flow ratio and nozzle position was $N = 0.255$ (fig. 7(b-2)).

Figure 8 (a cross plot of figures 7(a-1) and 7(b-1)) illustrates the effect of nozzle spacing on jet pump maximum efficiency for each area ratio. The maximum efficiency, after remaining relatively constant for nozzle spacings up to about 1 throat diameter for each configuration dropped off gradually as spacing was increased. This effect will be discussed later.

Comparison of Experiment and Theory

Plotted in figure 9 are theoretical curves for N and η as calculated by equations (13), (14), (34), and (35) (appendix B) for the fully inserted nozzle position. The loss factor K_t' used in equations (34) and (35) was determined after studying the total pressure surveys presented later in figures (14) to (16). Although this information would not be available to the designer, it was used in this instance to provide the most accurate measure of the potential usefulness of the modified theory. It is immediately evident that there is very little difference between the original conventional theory and the modified version. Furthermore, the experimental points, in general, compare closely to the conventional theory. At the best efficiency flow ratio the conventional theory predicted performance within about 3 percent.

One of the fundamental assumptions of the conventional theory is that nozzle spacing is zero. However, since jet pump performance changes little between nozzle spacings of 0 and 1 (figs. 7 and 8), the theory was also in general agreement with experiment in

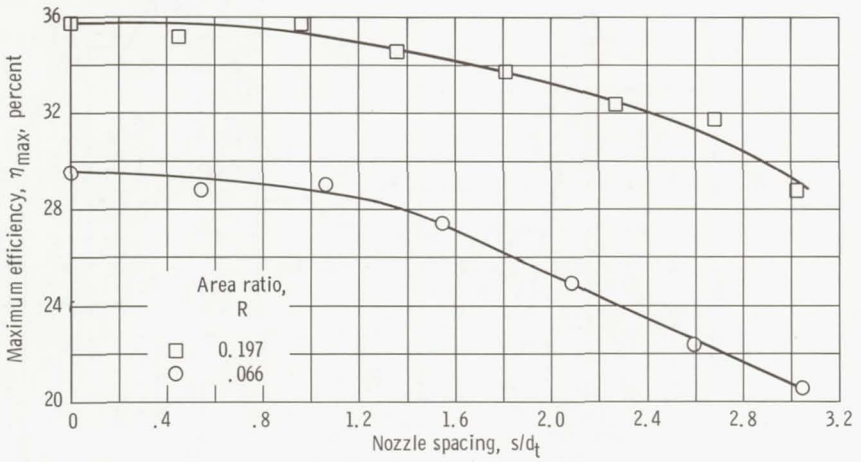

Figure 8. - Noncavitating jet pump performance. Effect of nozzle spacing on maximum efficiency.

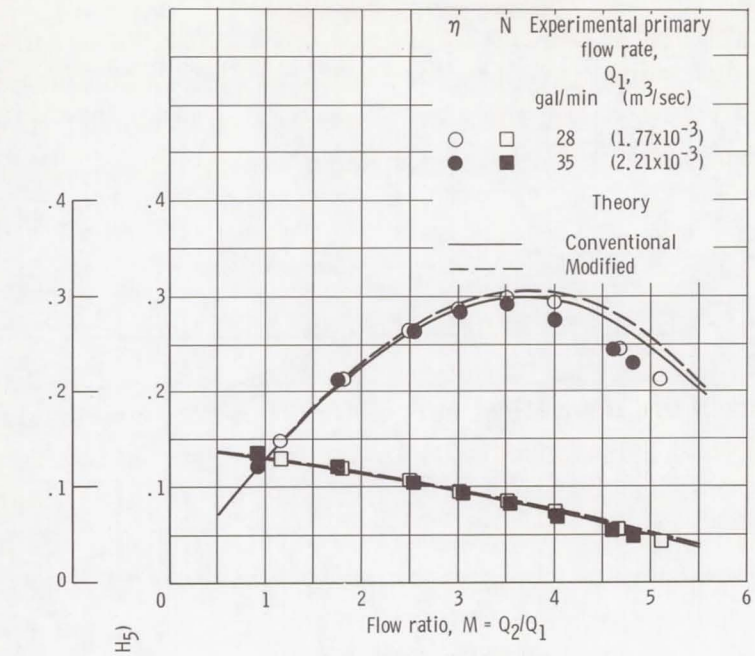

(a) Area ratio, R, 0.066.

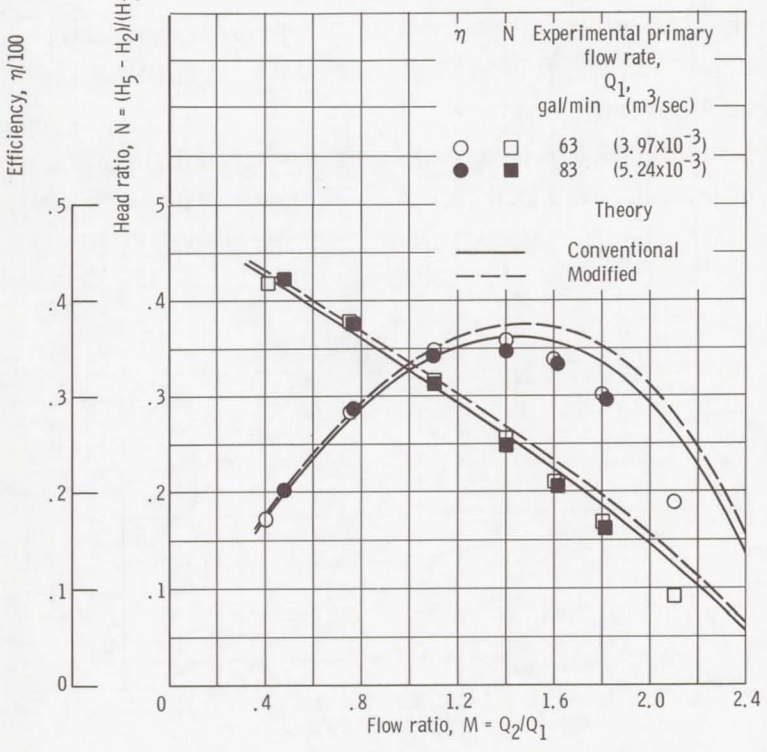

(b) Area ratio, R, 0.197.

Figure 9. - Comparison of theory with experimental points for fully inserted nozzle position ($s/d_t = 0$).

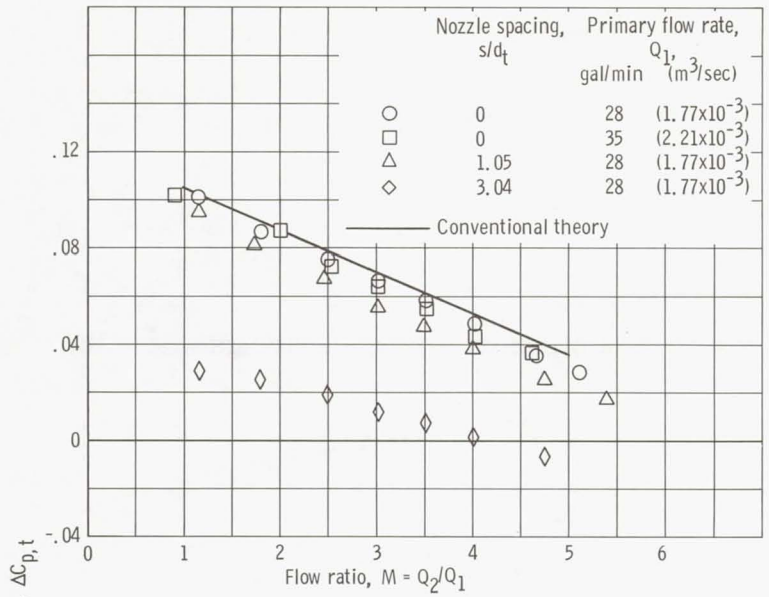

(a) Area ratio, R, 0.066.

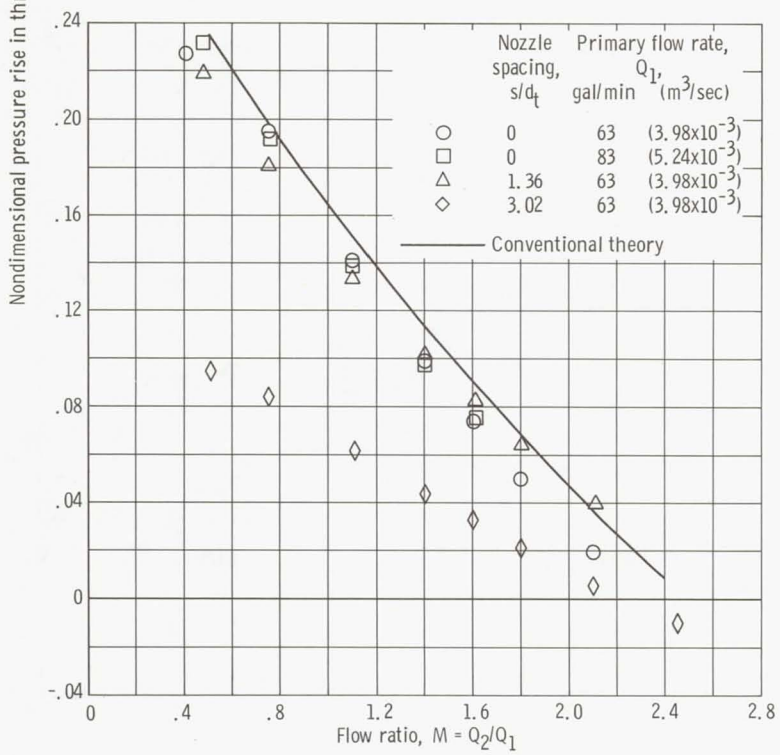

(b) Area ratio, R, 0.197.

Figure 10. - Nondimensional pressure rise in throat.

that range of s/d_t. As the nozzle is retracted, mixing occurs in the converging secondary inlet region as well as in the constant diameter throat. Therefore, it was not unexpected that at large nozzle spacings experimental performance did not agree with the theory.

An additional demonstration of the applicability of the conventional theory is shown in figure 10. With the same friction loss coefficients as were used in the calculations for figure 9, equation (28) was used to predict the pressure rise in the constant diameter throat. The theoretical nondimensional pressure rise in the throat $\Delta C_{p,t}$ is plotted against flow ratio in figure 10. Experimental values of the parameter at selected nozzle spacings for both area ratio pumps are also plotted in the figure. As in figure 9, the comparison between theory and experiment is good at zero and relatively low nozzle spacings, but they diverge significantly at large spacings where the premises of the theory are violated. A major effect of large nozzle spacings is a failure to achieve theoretically attainable pressure rise in the throat.

Mixing Characteristics

A better understanding of the internal fluid mechanics can be gained by an examination of the axial distributions of static pressure, and the radial surveys of total pressure.

Axial static pressure distributions. - Two distinct effects can be differentiated by an inspection of the static pressure distributions in the axial direction.

(1) Effect of nozzle position - A further experimental representation of the effect of nozzle spacing is shown in figure 11, a plot of the axial distribution of static pressure coefficient for both area ratios. Figure 11(a) presents data for an area ratio of $R = 0.066$ and for three different nozzle positions at the best efficiency flow ratio of $M = 3.5$. An important effect of nozzle spacing, evident at all flow ratios, is a general rise in the overall pressure level in the secondary inlet and throat entrance region as the nozzle is retracted from the throat entrance. This is due directly to an increase in annular area of the secondary inlet as the nozzle spacing is increased. Similar effects are exhibited by the $R = 0.197$ pump at three comparable nozzle spacings (fig. 11(b)). The major effect of a low-pressure level at very small nozzle spacings is a high susceptibility to cavitation. This is an important consideration because the best efficiency was obtained at a nozzle spacing of zero. If cavitation were to limit operation at this nozzle position, then some design compromises would have to be made. For this reason the zero nozzle spacing position should not be inflexibly categorized as the "optimum" nozzle position for this secondary inlet-throat-diffuser configuration.

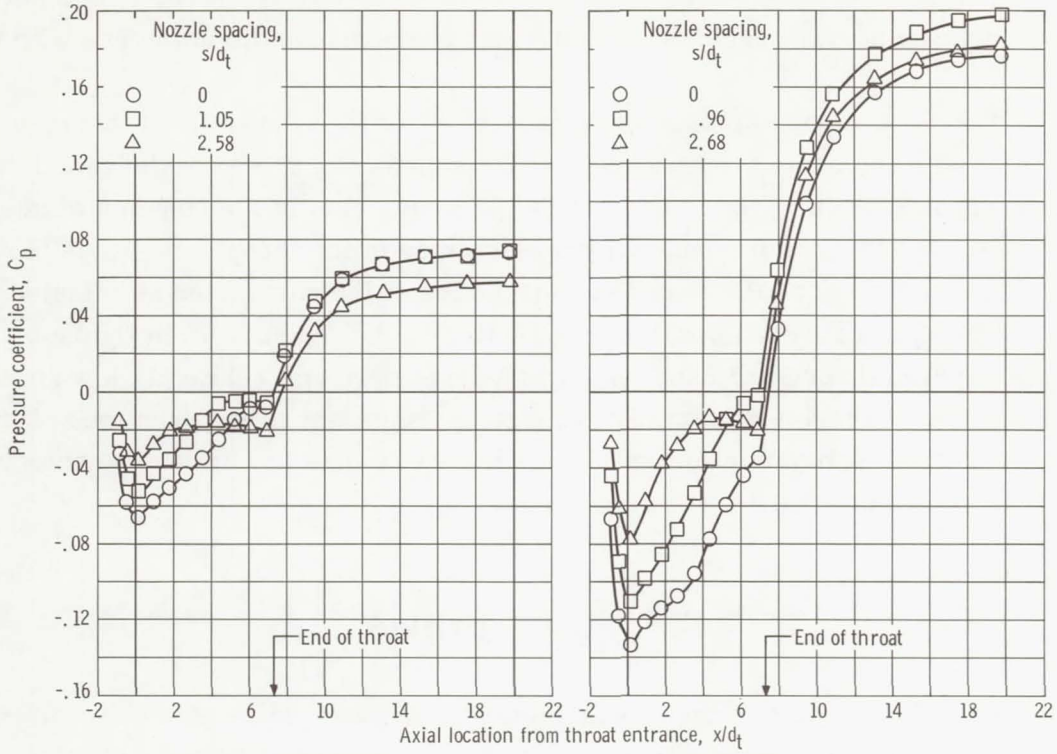

(a) Area ratio, R, 0.066; flow ratio, M, 3.5.

(b) Area ratio, R, 0.197; flow ratio, M, 1.4.

Figure 11. - Effect of nozzle position on axial static pressure distribution.

Mixing length can be equated with throat length only at zero nozzle spacing. When the nozzle is in a retracted position it is not practical to define an equivalent mixing length because of the unknown effects on the turbulent mixing of the pressure and velocity field in the secondary inlet region. The length of the throat should be sufficient to permit the static pressure to increase continually with length, but not so long as to cause static pressure to become constant or decrease due to friction losses. The length of throat necessary to permit static pressure to reach a maximum is plotted in figure 12 as a function of nozzle spacing for both area ratios. The curves represent the limit of static pressure increase in the throat for all flow ratios and are general in nature. The figure should not be interpreted as a plot of optimum or recommended throat lengths. What is significant about the figure is that the two area ratios demonstrate different static pressure trends in the throat. The static pressure reached a peak earlier in the throat for the smaller area ratio pump (R = 0.066). Another way of stating this is that a longer mixing length was required at all nozzle positions for the larger area ratio pump (R = 0.197). Therefore, it may be concluded that area ratio, as well as nozzle position, influences the length of throat required to complete mixing.

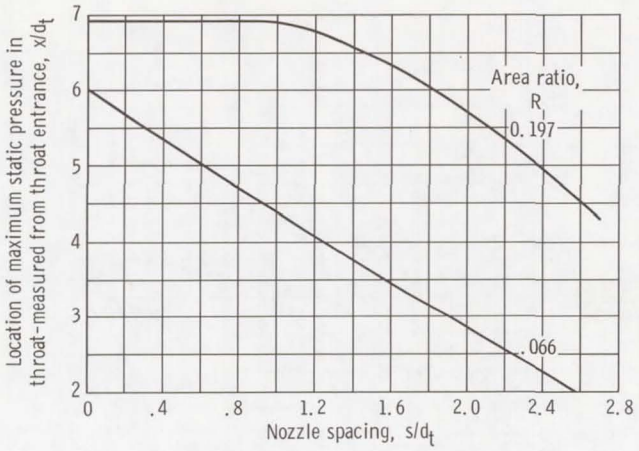

Figure 12. - Effect of nozzle spacing on limit of static pressure increase in throat.

(2) Effect of flow ratio - Comparisons of static pressure profiles for three flow ratios at $s/d_t = 0$ for both of the area ratios are presented in figure 13. The dashed lines mark the limits of static pressure increase in the throat. It can be seen that for the fully inserted nozzle position there is no significant effect of flow ratio on the axial position at which static pressure rise ceases. Similarly, no effect of flow ratio was demonstrated at the other nozzle positions for either area ratio.

It is quite clear from figure 13 that one major effect of flow ratio is a reduction in overall pressure level in the jet pump as flow ratio is increased. The natural consequence of this is a greater susceptibility to cavitation at high flow ratios.

Also apparent from figure 13 is the decrease in pressure rise in the throat, $(\Delta C_{p,t})$ as flow ratio is increased. This same effect was described earlier by equation (28) and figure 10.

Total pressure surveys. - A series of total pressure surveys, for both area ratios, are presented in figures 14 to 16. Axial static pressure distributions are included to aid interpretations. The total pressure surveys, conducted in the radial direction, were obtained at the same nozzle positions previously considered.

The normalized parameter $\mathscr{P}$ was obtained by dividing each local radial value of total pressure by the maximum value of total pressure (usually the midstream value). The normalized total pressure profile serves as a qualitative measure of the presence or absence of energy addition at a specified axial location. Total pressure surveys were

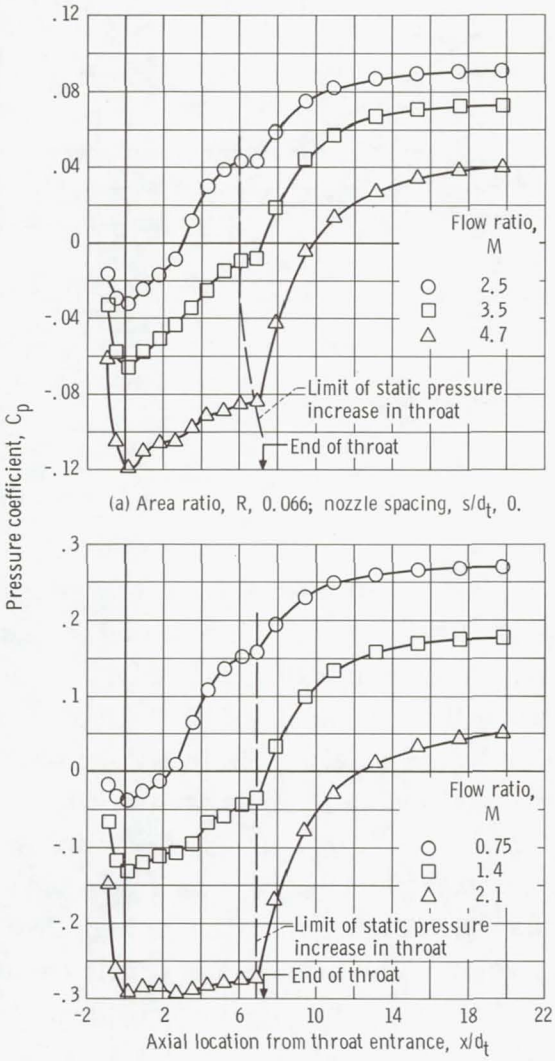

(a) Area ratio, R, 0.066; nozzle spacing, s/d_t, 0.

(b) Area ratio, R, 0.197; nozzle spacing, s/d_t, 0.

Figure 13. - Effect of flow ratio on axial static pressure distributions.

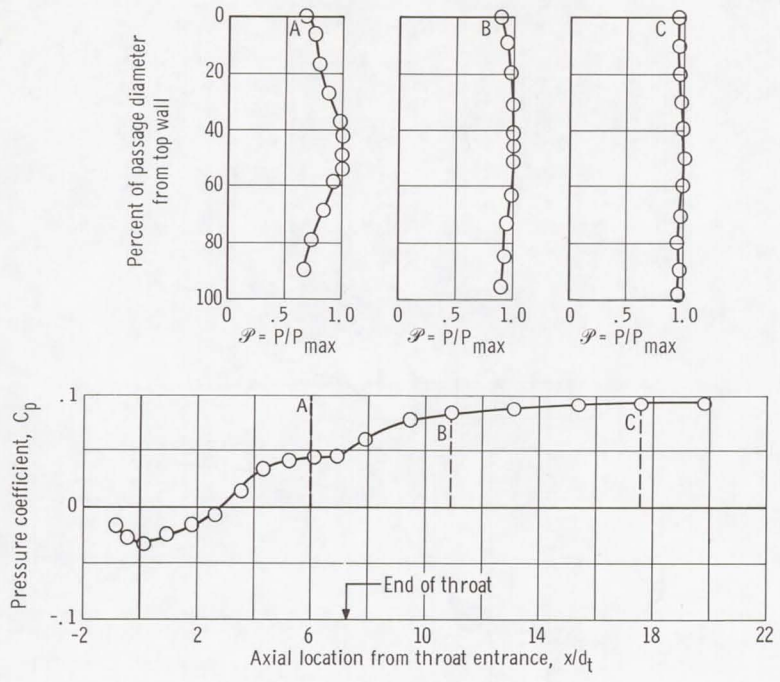

(a) Flow ratio, M, 2.5.

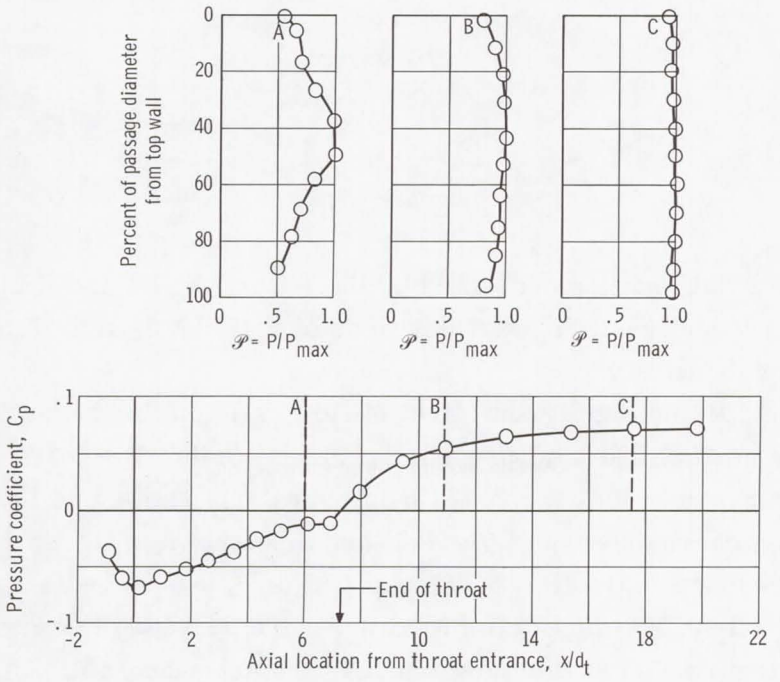

(b) Flow ratio, M, 3.5.

Figure 14. - Effect of flow ratio on mixing chracteristics. Area ratio, R, 0.066; nozzle spacing, s/d_t, 0.

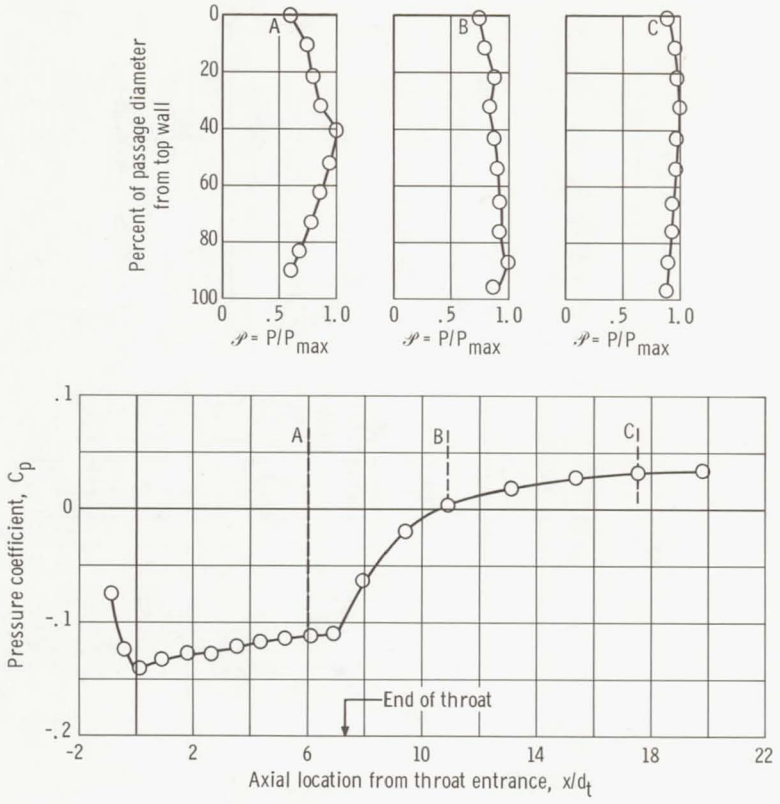

(c) Flow ratio, M, 5.0.

Figure 14. - Concluded.

conducted at three axial locations, denoted by the letters A, B, and C on the curves, and they correspond, respectively, to axial positions of 6.0, 10.9, and 17.5 throat diameters measured from the throat inlet.

Figure 14 reveals no significant effect of flow ratio on the mixing characteristics (inferred from the normalized total pressure profiles) in the R = 0.066 pump at $s/d_t = 0$. Other surveys in the R = 0.197 pump similarly showed no influence of flow ratio. As has been previously noted (fig. 12) and also shown in figure 14, the leveling off of the static pressure in the R = 0.066 pump at $s/d_t = 0$ suggests a completion of mixing by $x/d_t = 6.0$. However, the total pressure surveys of figure 14 show the existence of a mixing profile at this position. As the secondary fluid gains energy from the primary fluid through turbulent mixing it loses energy to friction. In this particular case (fully inserted nozzle position), at the end of the throat ($x/d_t = 7.25$) mixing is still proceeding, but the gain in energy due to mixing is offset by friction losses so that there is no net gain in static pressure.

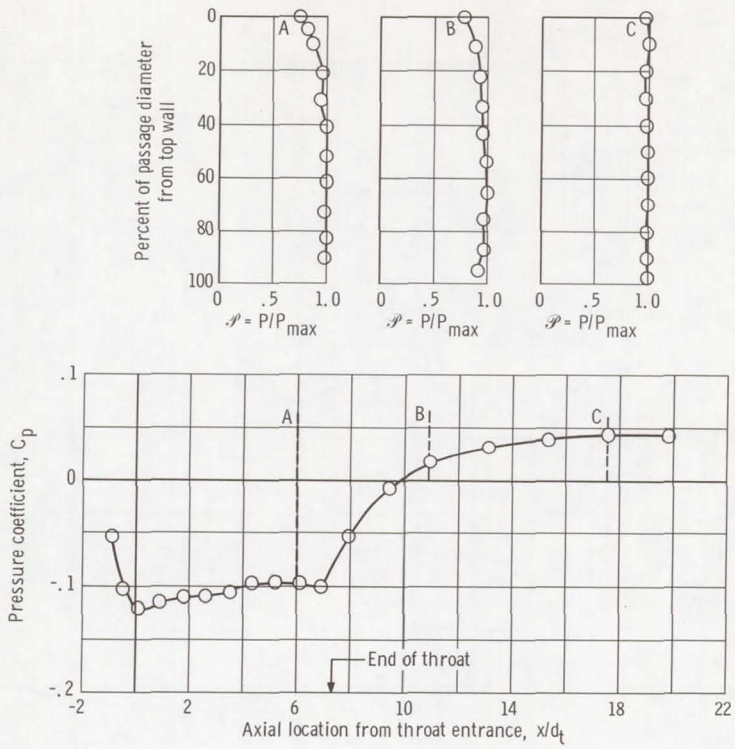

(a) Nozzle spacing, s/d_t, 1.05.

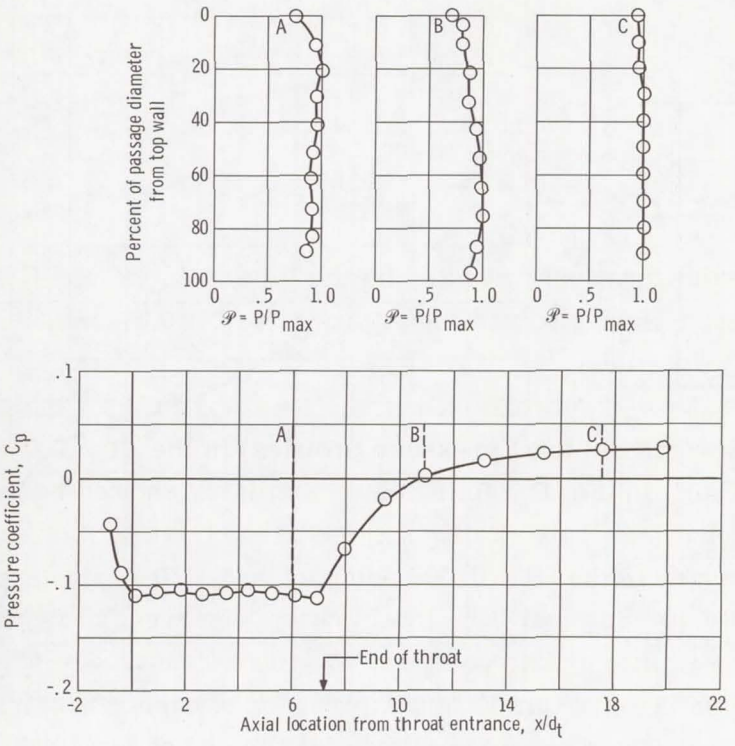

(b) Nozzle spacing, s/d_t, 2.58.

Figure 15. - Effect of nozzle position on mixing characteristics. Area ratio, R, 0.066; flow ratio, M, 5.0.

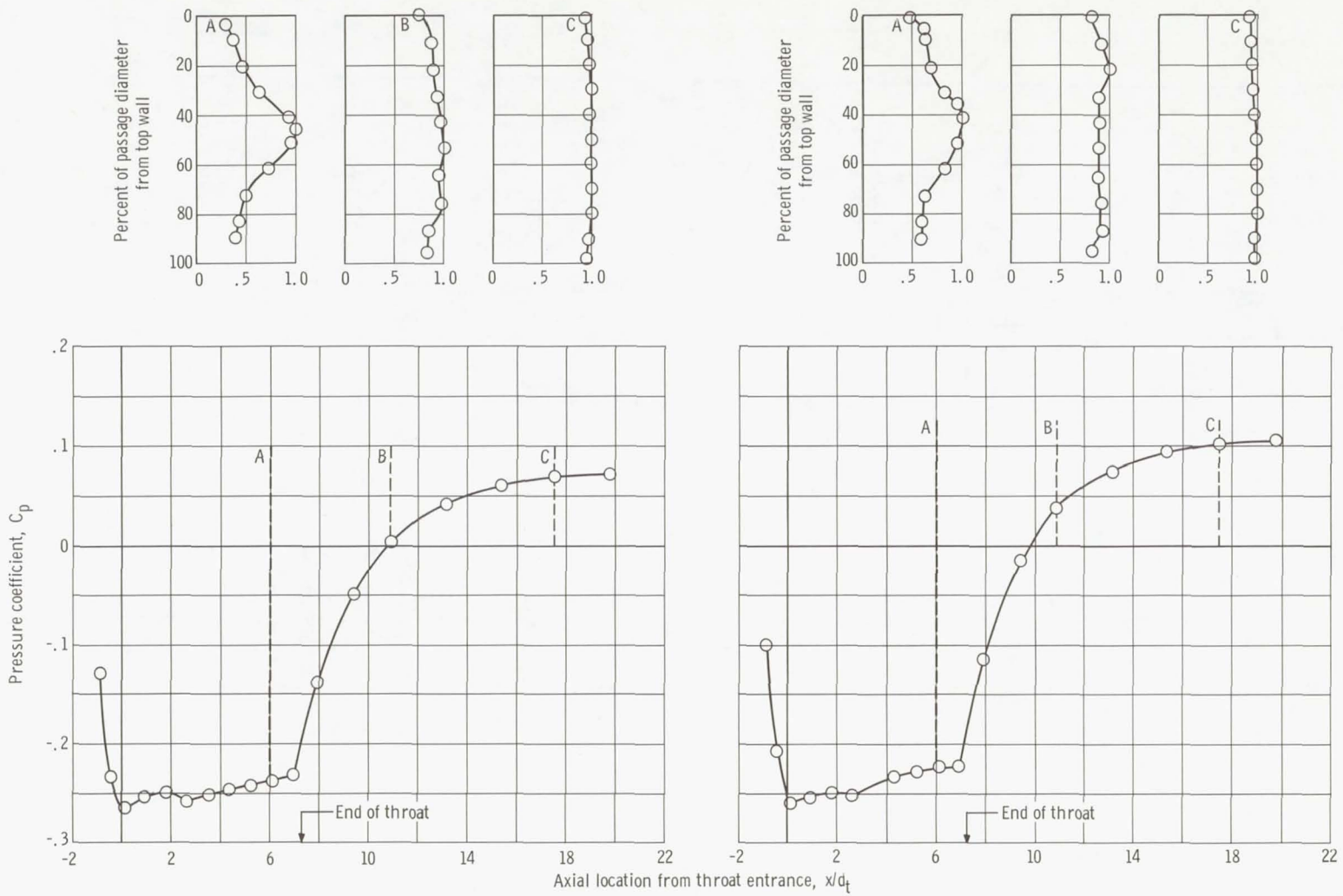

(a) Nozzle spacing, s/d_t, 0; flow ratio, M, 2.0.

(b) Nozzle spacing, s/d_t, 0.96; flow ratio, M, 2.1.

Figure 16. - Effect of nozzle position on mixing characteristics. Area ratio, R, 0.197.

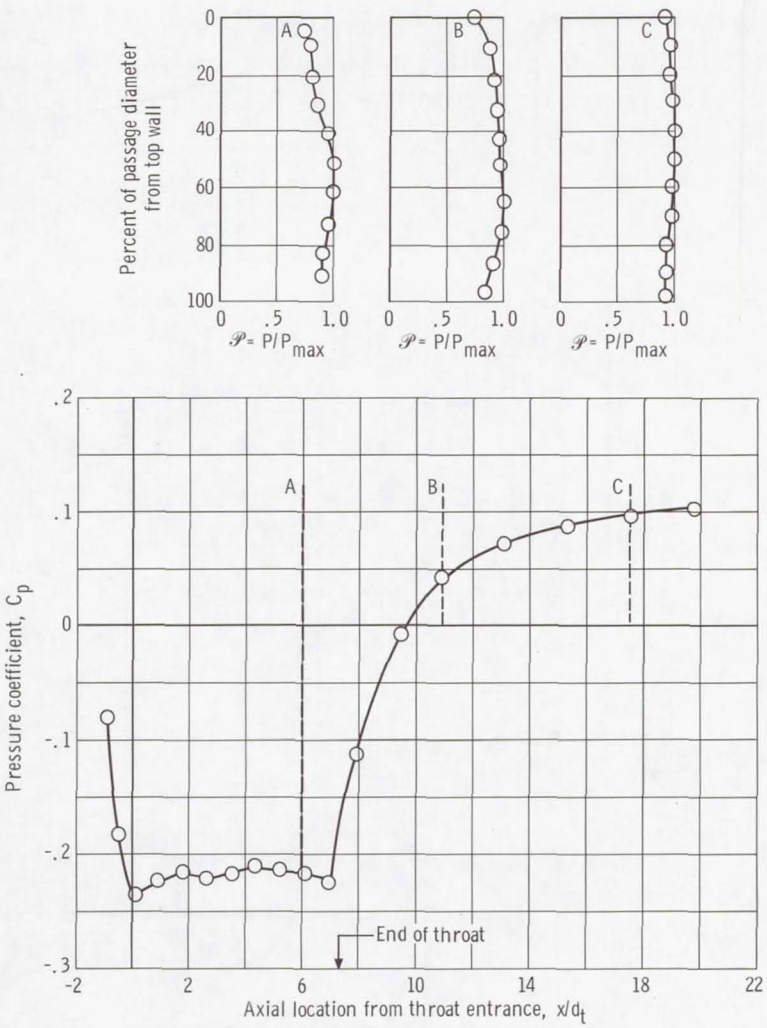

(c) Nozzle spacing, s/d_t, 2.68; flow ratio, M, 2.1.

Figure 16. - Concluded.

At other nozzle spacings of 1.05 and 2.58 diameters, the total pressure surveys for M = 5.0 indicate no substantial mixing profile at an axial location of $x/d_t = 6.0$ or beyond (fig. 15). Generally speaking, for R = 0.066, there appears to be no indication of a mixing profile at an axial location, $x/d_t = 10.9$ or beyond.

The surveys for R = 0.197 (fig. 16) demonstrate a more accentuated mixing profile at $x/d_t = 6.0$ for a zero nozzle spacing than did surveys for R = 0.066. Energy addition continued for the full length of the throat, and the profiles in the diffuser indicate no noticeable adverse effects of the nonuniform inlet profiles. At the 0.96 nozzle spacing (fig. 16(b)), mixing profiles at $x/d_t = 6.0$ are still present, but the rate of energy addition is insufficient to overcome frictional losses beyond $x/d_t = 6.0$. At nozzle spacings of 2.68 throat diameters (fig. 16(c)), little mixing is indicated by the surveys, and substantiating this, the static pressure profile shows a loss in pressure in the throat due to friction beginning at $x/d_t = 4.0$.

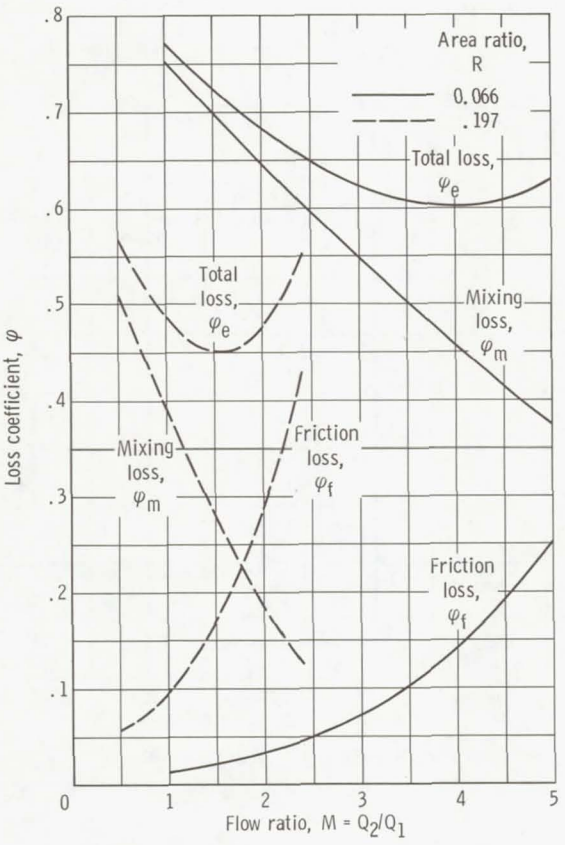

Figure 17. - Comparison of jet pump theoretical losses at two area ratios - conventional analysis.

The expressions for mixing, friction, and the sum of these (total) losses (eqs. (19), (24), and (25)) developed earlier are presented in graphical form in figure 17 for area ratios of R = 0.066 and 0.197. Values of K used in the formulas and their sources are given in appendix B. For either area ratio, it can be observed at low flow ratios that by

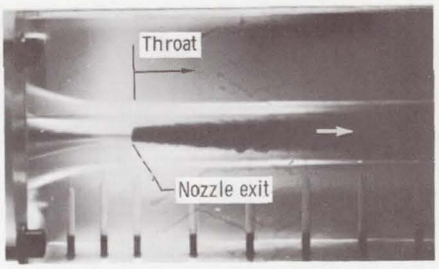

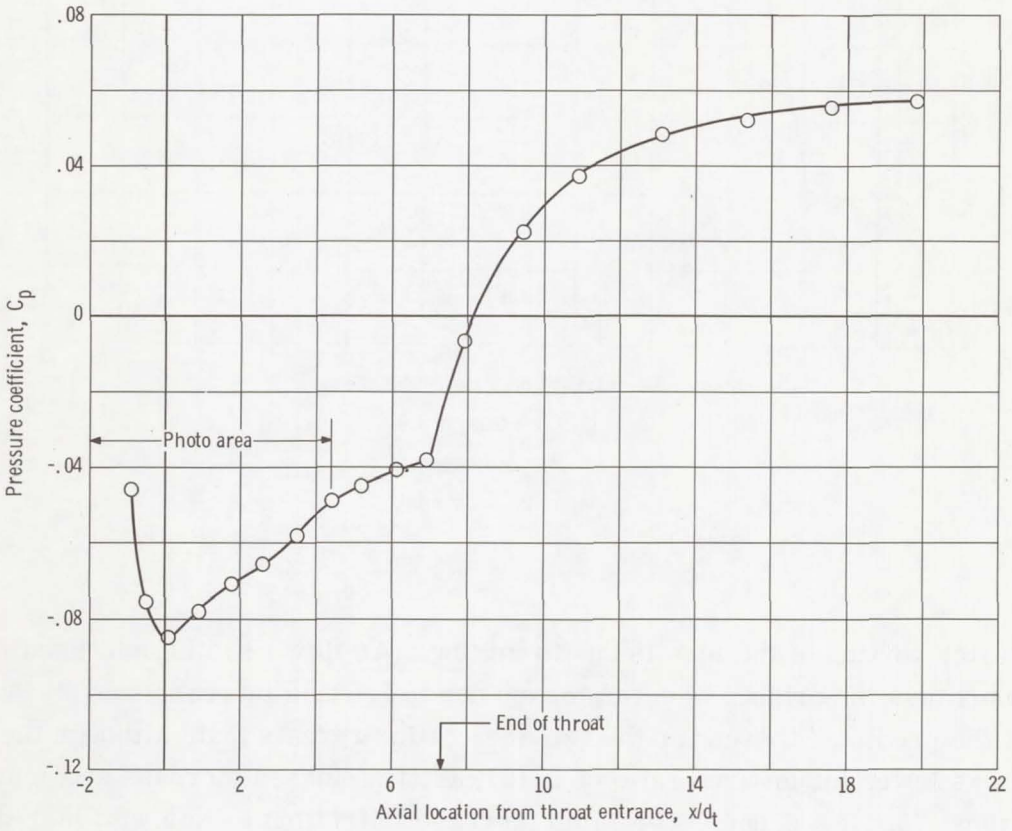

(a-1) Flow ratio, M, 3.9.

(a) Nozzle spacing, s/d_t, 0.

Figure 18. - Location of recirculation vortices. Area ratio, R, 0.066.

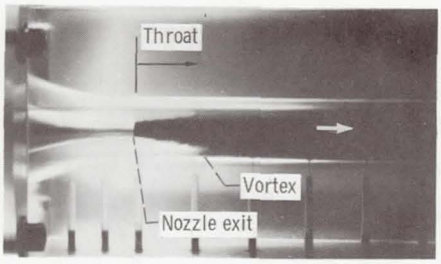

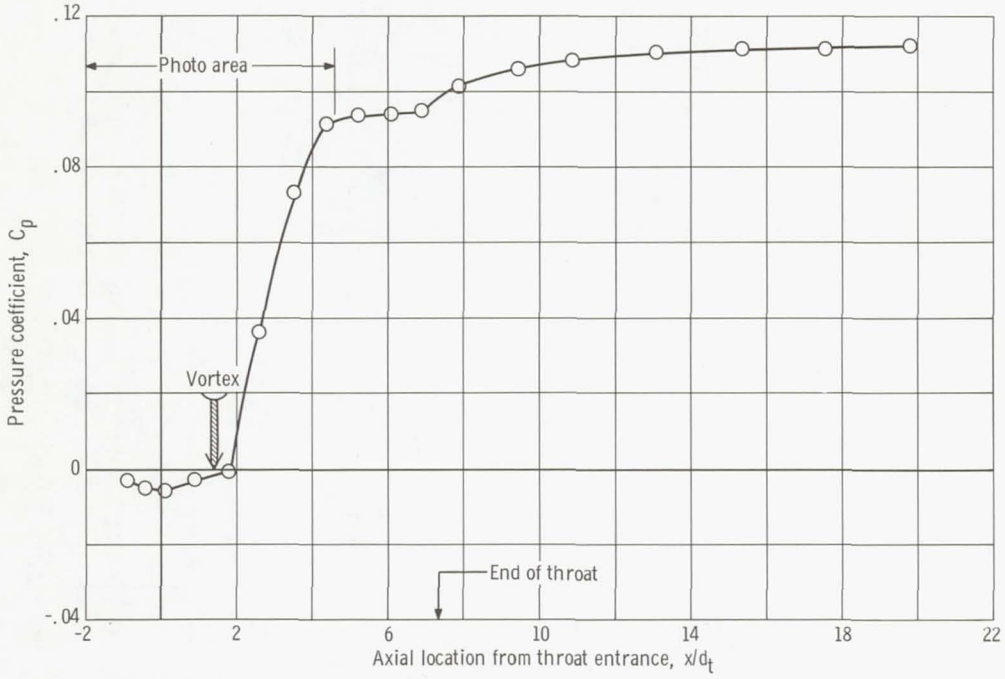

(a-2) Flow ratio, M, 1.0.

(a) Continued.

Figure 18. - Continued.

far the greater portion of the loss is due to mixing. As flow ratio is increased mixing loss becomes less important, whereas losses due to friction increase sharply. A comparison of the predicted losses for the two area ratios reveals that, although the loss due to mixing was lower for an area ratio of 0.197, friction losses increase at a much steeper rate than those for R = 0.066. The rapid increase in friction losses with increasing flow ratios in high-area-ratio pumps thus restricts the operating range to regions of low flow ratio. However, the level of overall losses in this range are lower than those for the R = 0.066 pump and therefore a higher operating efficiency will be obtained for the R = 0.197 pump.

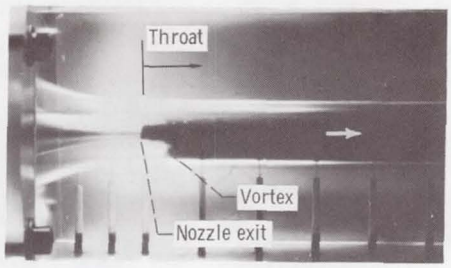

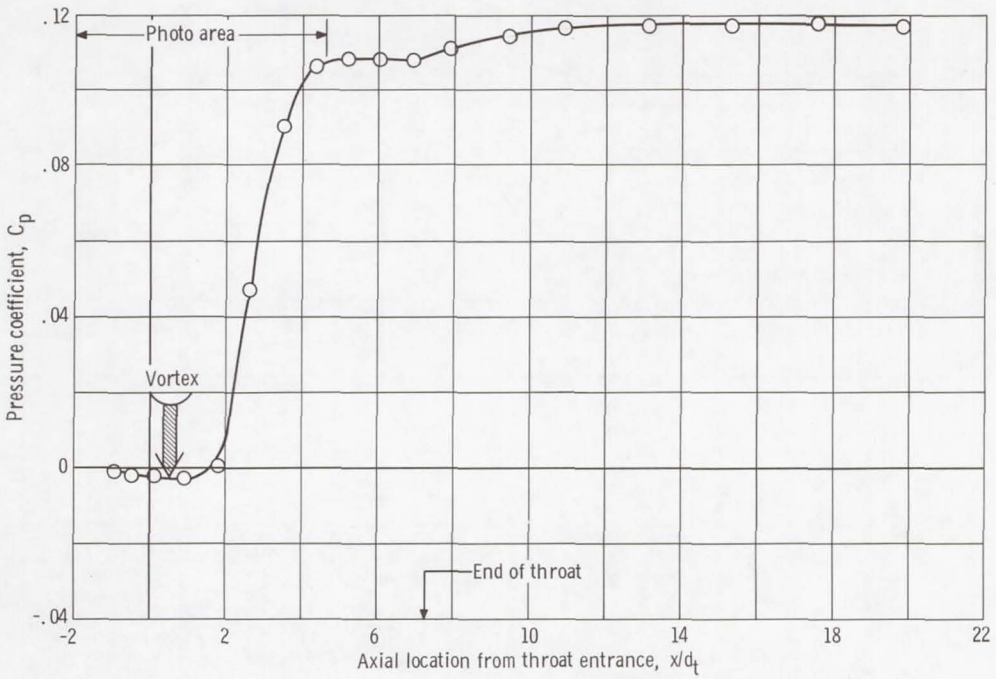

(a-3) Flow ratio, M, 0.6.

(a) Concluded.

Figure 18. - Continued.

Photographic studies were made of mixing patterns at several flow ratios using dye injected into the primary fluid upstream of the nozzle. Photographs of the flow for R = 0.066 at two nozzle spacings are presented in figure 18 with the associated static pressure distributions. At high flow ratios the angle of spread of the primary fluid core was very small (fig. 18(a-1)), which suggests a gradual diffusion of primary kinetic energy to the secondary stream (as indicated by the low mixing losses in fig. 17). As flow ratio is reduced, the pressure rise through the pump increases and the lower velocity secondary fluid encounters an increasingly adverse pressure gradient. In addition, the angle of spread of the primary fluid increases (cf., figs. 18(a-1) and (a-2)). Finally, a flow ratio

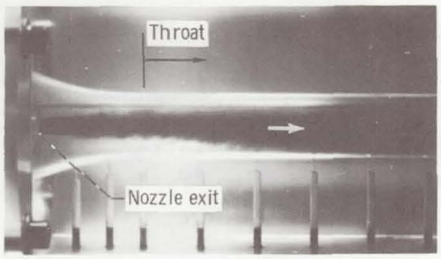

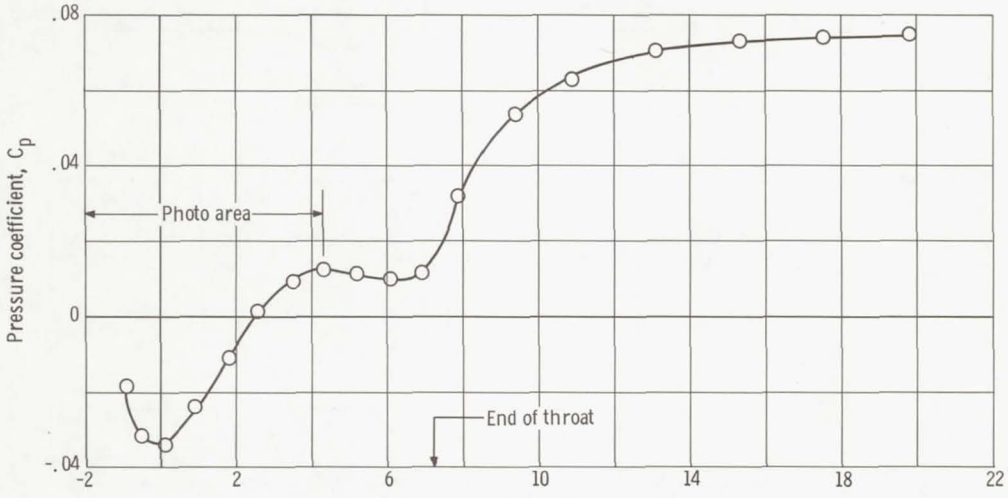

(b-1) Flow ratio, M, 3.1.

(b) Nozzle spacing, s/d_t, 1.54.

Figure 18. - Continued.

is reached (figs. 18(a-2) and (a-3)) at which the momentum of the secondary fluid cannot overcome the mixing chamber pressure gradient; thus, a region of separation and recirculation on the outer wall occurs in the secondary stream which leads to large-scale dissipation of energy.

Because the test section was top-lighted, reflections obscured the dye pattern above the nozzle in the photographs. The vortices, which can be identified in the lower portion of the photographs below the nozzle, were present symmetrically around the flow passage.

Thus, the high mixing losses predicted by theory at low flow ratios (eq. (19) and fig. 17) and identified by low efficiencies are seen to be due to large areas of recirculation in the secondary stream. The positions of the recirculation vortices, as determined from the photographs, have been denoted on the (fig. 18(a)) plot of axial distribution of

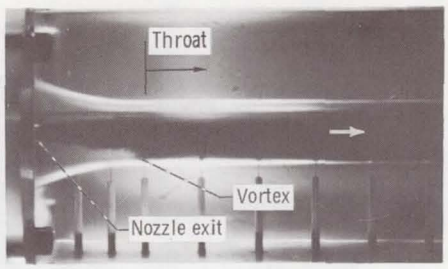

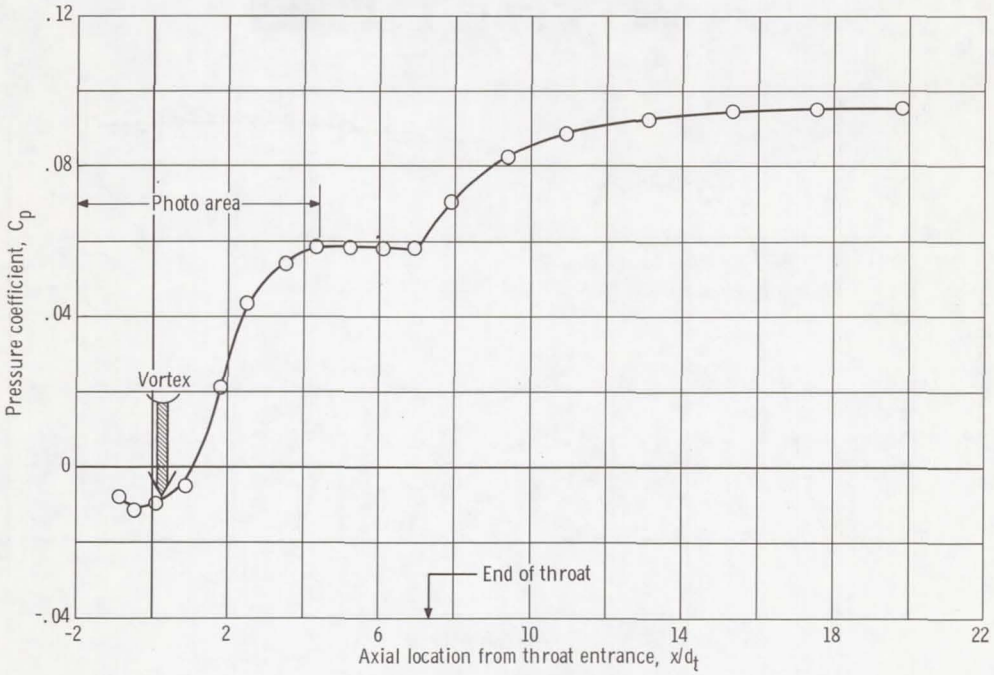

(b-2) Flow ratio, M, 2.1.

(b) Continued.

Figure 18. - Continued.

pressure coefficient C_p and in all cases occur at the leading edge of the region of steep pressure gradient.

The same flow mechanisms were operative at nozzle spacings greater than zero. Figure 18(b-1) depicts a condition of moderate throat pressure gradient and mixing losses for a nozzle spacing of $s/d_t = 1.54$. A steep pressure gradient and a vortex appears near the wall in figure 18(b-2). And finally, at a flow ratio of $M = 1.1$ (fig. 18(b-3)), a very steep pressure gradient begins to force reversal in flow direction of the secondary fluid before it reaches the throat entrance.

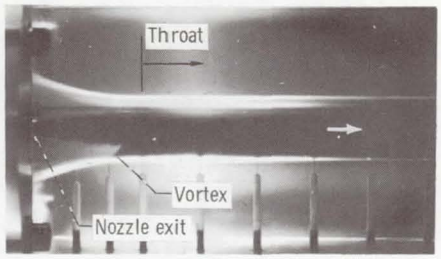

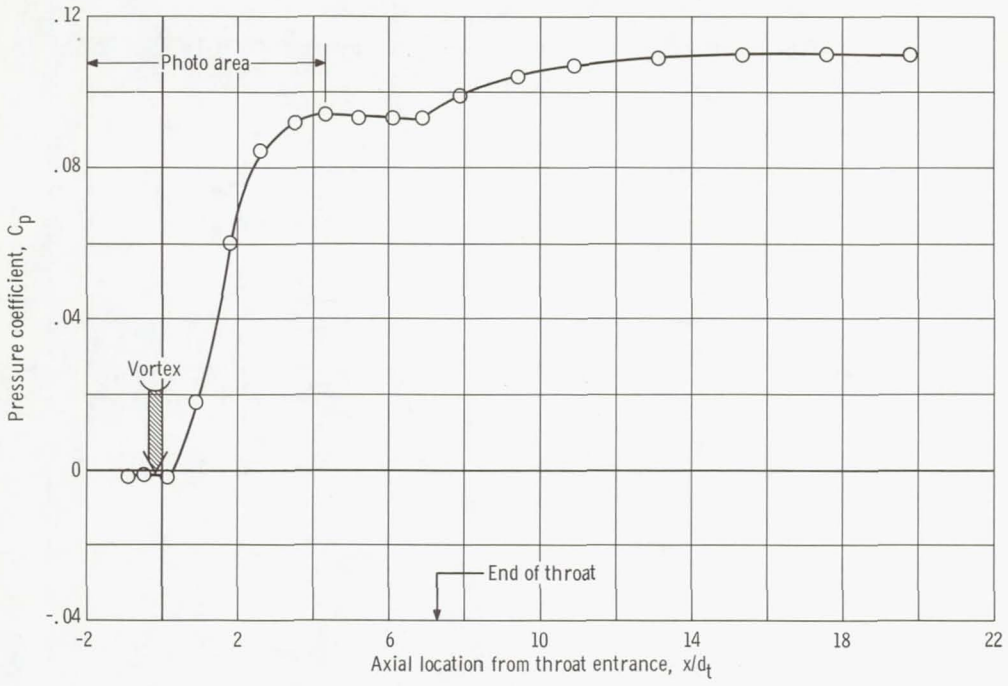

(b-3) Flow ratio, M, 1.1.

(b) Concluded.

Figure 18. - Concluded.

CONCLUDING REMARKS

As has been noted, determination of optimum geometrical configurations is an arduous task because of the large number of geometrical variables and their interrelations. Since one of the primary objectives of this investigation was to achieve a better understanding of some of the flow mechanisms of jet pumps, the test pump was not designed with optimum performance as the prime consideration. Therefore, the particular combination of geometrical components tested in this investigation should not necessarily be

regarded as an "optimum" combination. Furthermore, in analyzing the results it should be remembered that due to the interdependency of components attempts to separate the performance of parameters such as throat length, nozzle position, or diffuser angle from each other, and from overall performance, can be misleading. However, some general comments can be made about the configurations tested in this investigation.

THROAT LENGTH

The throat length of 7.25 diameters appeared to be sufficient, if not too long under some conditions. The fact that best efficiency was achieved at zero nozzle spacing for both area ratios indicates more throat mixing length was not required. That is, provision of more mixing length by retraction of the nozzle did not result in performance improvements. Consequently, it appears that a shorter throat length, perhaps 5 or 6 diameters in length, would contribute to improved performance.

One additional consideration to be noted is that the mixing length requirements of the two area ratio configurations showed a definite difference. Total pressure surveys and static pressure profiles indicated that the $R = 0.066$ pump required less throat length to complete mixing than the $R = 0.197$ pump.

NOZZLE SPACING

The effect of nozzle spacing on performance is directly related to throat length, and to a lesser degree to secondary inlet contour, and thus cannot be defined in an absolute sense. In the configurations under discussion, both nozzles displayed similar characteristics with respect to spacing, but performance deteriorated more rapidly with increased spacing for $R = 0.066$ than for $R = 0.197$. This apparent effect of area ratio on nozzle spacing is simply the same effect of area ratio on required mixing length discussed in the previous paragraph. Less mixing length was required for the $R = 0.066$ pump and therefore, as the nozzle was retracted, the $R = 0.066$ pump performance deteriorated more rapidly due to frictional losses in the throat.

DIFFUSER GEOMETRY

It was pointed out earlier that diffuser performance is dependent on the shape of the inlet velocity profile, and therefore related to the length of the throat in a jet pump. If mixing is not completed at the end of the throat there is danger of separation in the dif-

fuser. For the tests reported herein the total pressure surveys and static pressure profiles showed no evidence of separation at any of the flow conditions. However, the static pressure profiles (C_p against x/d_t) indicated only a small gain in static pressure beyond an x/d_t position of 15 (diffuser area ratio of 4.6), which indicates that the remainder of the diffuser was building friction losses at a faster rate than it was recovering static pressure. Thus, when matched with a relatively long throat, a diffuser included angle of $8^{\circ}6'$ (0.141 rad) performed satisfactorily, but nothing was gained by using a diffuser having an outlet- to inlet-area ratio in excess of 5. This substantiates the recommendations of reference 13, but it should be added that different, and probably poorer, overall jet pump performance would result if the same diffuser were to be matched with a shorter throat.

OVERALL PERFORMANCE

The maximum efficiency values reported in the jet pump literature are plotted in figure 19 as a function of area ratio. Also plotted in this figure, as solid points, are the maximum efficiencies obtained in this investigation. These peak efficiencies of 35.7 and 29.5 percent recorded at area ratios of 0.197 and 0.066, respectively, compare quite favorably with efficiencies reported to date in the literature, especially for R = 0.066.

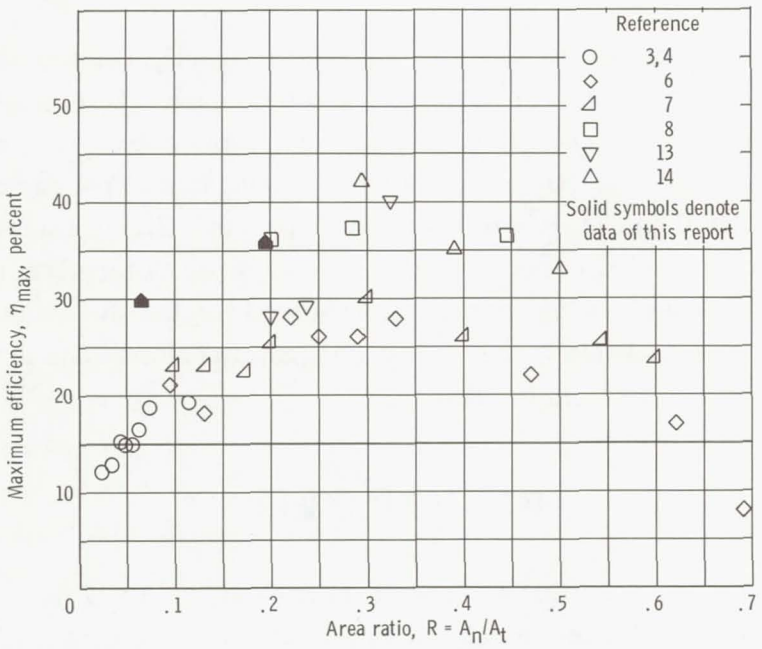

Figure 19. - Maximum reported jet pump efficiencies as function of area ratio.

It may therefore be concluded that, even though there was not a perfect matching of geometrical components, the particular combination used did have merit and can serve as a basis for future designs.

The low efficiencies measured at low flow rates were found to be due to inefficient mixing, which cannot be avoided. However, the low efficiencies measured at high flow ratios were found to be due largely to frictional losses. The losses in this flow regime can be minimized by using internally smooth components.

SUMMARY OF RESULTS

The performance of two jet pumps having low nozzle- to throat-area ratios was evaluated in a water facility and compared to theoretically predicted performance. The two jet pumps consisted of a single test section and either of two nozzles. The throat diameter of the test section was 1.35 inch (3.43 cm), the throat length 7.25 diameters, and the diffuser included angle $8^{o}6'$ (0.141 rad). The two nozzles had exit diameters corresponding to nozzle- to throat-area ratios of 0.066 and 0.197. Each nozzle was operated at several spacings of the nozzle exit upstream from the throat entrance over a range of from 0 to 3 throat diameters.

The investigation yielded the following principal results:

(1) For an area ratio of 0.066, a maximum measured efficiency of 29.5 percent was achieved at a zero nozzle spacing, and at a flow ratio of 3.5. The head ratio corresponding to this flow ratio and nozzle position was 0.084.

For an area ratio of 0.197, a maximum efficiency of 35.7 percent was achieved, also at a zero nozzle spacing, and at a flow ratio of 1.4. The head ratio corresponding to this flow ratio and nozzle position was 0.255.

(2) The throat length required to complete mixing was found to be related to area ratio as well as to nozzle spacing. Longer mixing lengths were necessary for the $R = 0.197$ configuration. For both area ratios, however, it appeared probable that a reduction in length of the throat to 5 or 6 diameters would improve performance.

(3) The zero nozzle spacing was found to be most efficient for both area ratio pumps because of the relatively long throat. Performance at maximum efficiency levels was maintained for both area ratio pumps over the range of nozzle spacings of 0 to 1 throat diameter, but performance decreased at larger spacings. However, due to increased susceptibility to cavitation at the zero nozzle spacing position, this nozzle position should not be inflexibly regarded as the "optimum" position for this configuration.

(4) Even though the diffuser included angle of $8^{o}6'$ (0.141 rad) was slightly in excess of recommended values for jet pump applications, no adverse effects were apparent. This is attributed to the existence of a relatively long throat which provided acceptable inlet

velocity profiles to the diffuser. However, the use of a diffuser having an outlet- to inlet-area ratio in excess of 5.0 was judged unnecessary.

(5) At small nozzle spacings (up to 1 throat diameter), a conventional one-dimensional analysis predicted performance within about 3 percent at the best efficiency flow ratio. A modified theory, which attempted to account for the effect of the mixing profile in the throat, required more computational effort and did not improve correlation with experimental performance.

(6) Low efficiencies exhibited at low flow ratios are due to inefficient mixing, whereas low efficiencies at high flow ratios are due largely to frictional losses.

Lewis Research Center,
National Aeronautics and Space Administration,
Cleveland, Ohio, September 21, 1967,
128-31-06-28-22.

APPENDIX A

SYMBOLS

A	area, ft^2 (m^2)
C_p	pressure coefficient, $(p_x - p_2)/\gamma(V_n^2/2g)$
$\Delta C_{p,t}$	pressure coefficient rise in throat, $(p_4 - p_3)/\gamma(V_n^2/2g)$
d	diameter, in. (cm)
E	time rate of energy term ft-lb_{force}/sec (W)
f	Darcy friction factor
F	force, lb_{force} (N)
g	local acceleration due to gravity, 32.163 ft/sec^2 (9.803 m/sec^2)
g_c	dimensional constant, 32.174 (ft)(lb_{mass})/(sec^2)(lb_{force}) (1.0 (m)(kg)/(sec^2)(N))
h	static head of fluid, p/γ, ft (m)
H	total head of fluid, P/γ, ft (m)
K	friction loss coefficient
K_t'	throat friction loss coefficient in region of throat in which mixing is proceeding - modified theory (fig. 21)
K_t''	throat friction loss coefficient in region of throat in which mixing has been completed - modified theory (fig. 21)
l	throat length, in. (cm)
L	length, in. (cm)
L'	length of throat in which mixing is proceeding - modified theory (fig. 21), in. (cm)
L''	length of throat in which mixing has been completed - modified theory (fig. 21), in. (cm)
M	flow ratio, Q_2/Q_1
N	head ratio, $(H_5 - H_2)/(H_1 - H_5)$
p	static pressure, lb_{force}/ft^2 (N/m^2)
P	total pressure, lb_{force}/ft^2 (N/m^2)
$\mathscr{P}$	normalized total pressure, P/P_{max}
Q	volumetric flow rate, gal/min (m^3/sec)
R	area ratio, A_n/A_t
s	axial spacing of primary nozzle exit from throat entrance, in. (cm)
V	velocity, ft/sec (m/sec)
w	mass flow rate, lb_{mass}/sec (kg/sec)
x	axial distance from throat entrance, in. (cm)
β	diffuser included angle, deg (rad)

γ specific weight, $\rho(g/g_c)$, lb_{force}/ft^3 (N/m^3)

η efficiency, MN

ρ fluid density, lb_{mass}/ft^3 (kg/m^3)

φ dimensionless loss factor

Subscripts:

d diffuser

f friction

l total loss

m mixing

n primary nozzle exit plane

p primary nozzle

s secondary fluid inlet

t throat

ts test section

x linear position measured in axial direction from throat entrance

1 primary fluid

2 secondary fluid

3 location at throat inlet

4 location at throat exit

5 location at jet pump discharge

APPENDIX B

DEVELOPMENT OF JET PUMP EQUATIONS

The equations of jet pump performance are derived from successive applications of the energy, momentum, and continuity relations to the flow in the several components of the jet pump. Certain preliminary assumptions are necessary:

(1) Primary and secondary fluids are incompressible and of equal density.

(2) Spacing of the nozzle exit from the throat entrance is zero ($s/d_t = 0$).

(3) Nozzle wall thickness at exit is zero ($A_3 = A_t - A_n$).

(4) Mixing is complete at the throat exit.

CONVENTIONAL ANALYSIS

Performance Parameters

Application of the energy equation

$$\frac{p_{inlet}}{\gamma} + \frac{V_{inlet}^2}{2g} = \frac{p_{outlet}}{\gamma} + \frac{V_{outlet}^2}{2g} + \frac{p_{friction}}{\gamma}$$

to each component yields the following expressions for the primary nozzle, secondary inlet, and diffuser (see fig. 20 for nomenclature):

Primary nozzle, stations 1 to n:

$$P_1 - p_n = \frac{\gamma V_n^2}{2g}(1 + K_p) \tag{1}$$

where

$$K_p = \frac{p_{f,p}}{\gamma V_n^2/2g}$$

Secondary inlet, stations 2 to 3:

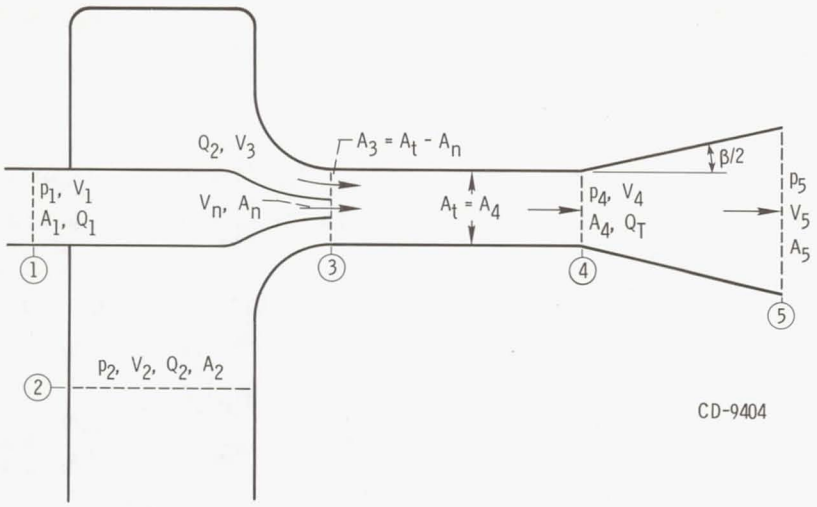

Figure 20. - Jet pump nomenclature.

$$P_2 - p_3 = \frac{\gamma V_3^2}{2g}(1 + K_s) \tag{2}$$

where

$$K_s = \frac{p_{f,s}}{\gamma V_3^2/2g}$$

Diffuser, stations 4 to 5:

$$P_5 - p_4 = \frac{\gamma V_4^2}{2g}(1 - K_d) \tag{3}$$

where

$$K_d = \frac{p_{f,d}}{\gamma V_4^2/2g}$$

The head ratio N and efficiency η are defined by

$$N = \frac{H_5 - H_2}{H_1 - H_5} = \frac{P_5 - P_2}{P_1 - P_5} \tag{4}$$

and

$$\eta = MN \tag{5}$$

The numerator of N, $P_5 - P_2$, is given by

$$P_5 - P_2 = (P_5 - p_4) + (p_4 - p_3) - (P_2 - p_3)$$

where

$$P_5 - p_4 = \frac{\gamma V_4^2}{2g}(1 - K_d)$$

Application of the continuity equation

$$V_4 = \frac{w_t}{\rho A_t}$$

and the geometrical and flow relations (where $w_t = w_1 + w_2$).

$$M = \frac{Q_2}{Q_1} \tag{6}$$

$$R = \frac{A_N}{A_T} \tag{7}$$

yield

$$V_4 = R(1 + M)V_n$$

and

$$P_5 - p_4 = \frac{\gamma}{2g} R^2 (1 + M)^2 V_n^2 (1 - K_d) \tag{8}$$

Applying the momentum equation across the throat gives the static pressure rise in throat, $p_4 - p_3$:

$$p_4 - p_3 = \frac{w_1 V_n}{g_c A_t} + \frac{w_2 V_3}{g_c A_t} - \frac{w_t V_4}{g_c A_t} - \gamma h_{f,t}$$

An expression for friction loss in the throat $h_{f,t}$ is obtained by assuming mixing to be complete at the throat exit and pipe flow friction loss relations to apply along the full length of the throat:

$$h_{f,t} = K_t \frac{V_4^2}{2g}$$

where

$$K_t = f \frac{l}{d_t}$$

$$h_{f,t} = K_t \frac{V_n^2}{2g} R^2 (1 + M)^2$$

So,

$$p_4 - p_3 = \frac{\gamma V_n^2}{2g} \left[2R + \frac{2R^2 M^2}{1 - R} - (2 + K_t) R^2 (1 + M)^2 \right] \tag{9}$$

Pressure difference across secondary inlet region $(P_2 - p_3)$ is

$$P_2 - p_3 = P_2 - p_n$$

If station n = station 3,

$$P_2 - p_3 = \frac{\gamma V_n^2}{2g}(1 + K_s)\frac{M^2R^2}{(1 - R)^2} \tag{10}$$

The final expression for the numerator of N is

$$P_5 - P_2 = \frac{\gamma V_n^2}{2g}\left[2R + \frac{2R^2M^2}{1 - R} - (1 + K_t + K_d)R^2(1 + M)^2 - (1 + K_s)\frac{R^2M^2}{(1 - R)^2}\right] \tag{11}$$

while the denominator of N, $(P_1 - P_5)$, is

$$P_1 - P_5 = (P_1 - p_3) - (P_2 - p_3) - (P_5 - P_2)$$

or

$$P_1 - P_5 = \frac{\gamma V_n^2}{2g}\left[1 + K_p - 2R - \frac{2R^2M^2}{1 - R} + R^2(1 + M)^2(1 + K_t + K_d)\right] \tag{12}$$

The final expression for head ratio

$$N = \frac{P_5 - P_2}{P_1 - P_5}$$

is

$$N = \frac{2R + \frac{2R^2M^2}{1 - R} - (1 + K_t + K_d)R^2(1 + M)^2 - (1 + K_s)\frac{R^2M^2}{(1 - R)^2}}{1 + K_p - 2R - \frac{2R^2M^2}{1 - R} + R^2(1 + M)^2(1 + K_t + K_d)} \tag{13}$$

The jet pump efficiency ($\eta = MN$) is

$$\eta = \frac{2RM + \frac{2R^2M^3}{1 - R} - (1 + K_t + K_d)R^2M(1 + M)^2 - (1 + K_s)\frac{R^2M^3}{(1 - R)^2}}{1 + K_p - 2R - \frac{2R^2M^2}{1 - R} + R^2(1 + M)^2(1 + K_t + K_d)} \tag{14}$$

Dimensionless Loss Expressions

Through algebraic manipulation of the energy, momentum, and continuity principles, dimensionless parameters may be derived which express losses in the jet pump due to mixing and friction.

The rate of energy loss due to mixing is obtained as follows. Applying the momentum equation across the throat yields

$$\frac{w_1V_n}{g_c} + \frac{w_2V_3}{g_c} + p_3A_t = \frac{w_tV_4}{g_c} + p_4A_t + F_{f,t}$$

or

$$p_4 - p_3 = \frac{w_1V_n}{g_cA_t} + \frac{w_2V_3}{g_cA_t} - \frac{w_tV_4}{g_cA_t} - \frac{F_{f,t}}{A_t} \tag{15}$$

Applying the energy equation across the throat gives

$$\frac{w_1p_3}{\rho} + \frac{w_1V_n^2}{2g_c} + \frac{w_2p_3}{\rho} + \frac{w_2V_3^2}{2g_c} = \frac{w_tp_4}{\rho} + \frac{w_tV_4^2}{2g_c} + E_m + E_{f,t}$$

or

$$p_4 - p_3 = \frac{w_1}{w_t}\frac{\rho V_n^2}{2g_c} + \frac{w_2}{w_t}\frac{\rho V_3^2}{2g_c} - \frac{\rho V_4^2}{2g_c} - \frac{\rho E_m}{w_t} - \frac{\rho E_{f,t}}{w_t} \tag{16}$$

When the two expressions for $p_4 - p_3$ are equated and the continuity equation and expression for friction loss in the throat is applied,

$$w_t = \rho_t A_t V_4$$

and

$$\Delta p_{f,t} = \frac{F_{f,t}}{A_t} = \frac{\rho E_{f,t}}{w_t}$$

the result is

$$E_m = w_1 \frac{(V_n - V_4)^2}{2g_c} + \frac{w_2 (V_3 - V_4)^2}{2g_c} \tag{17}$$

which is the rate of energy loss in the throat due to mixing. Dividing equation (17) by

$$E_n = \frac{w_1 V_n^2}{2g_c} \tag{18}$$

gives the dimensionless mixing energy loss φ_m:

$$\varphi_m = \frac{E_m}{E_n} = 1 + R^2 (1 + M)^3 - 2R (1 + M) + \frac{M^3 R^2}{(1 - R)^2} - \frac{2M^2 R^2 (1 + M)}{(1 - R)} \tag{19}$$

The rate of energy loss due to friction is found as follows:

Primary nozzle loss:

$$E_p = K_p w_1 \frac{V_n^2}{2g_c}$$

Secondary inlet loss:

$$E_s = K_s w_2 \frac{V_3^2}{2g_c}$$

Throat-diffuser loss:

$$E_t = K_t w_t \frac{V_4^2}{2g_c}$$

$$E_d = K_d w_t \frac{V_4^2}{2g_c}$$

$$E_{td} = E_t + E_d = (K_t + K_d)\, w_t \frac{V_4^2}{2g_c}$$

Overall friction loss:

$$E_f = E_p + E_s + E_t + E_d$$

Dividing the previous equation by $E_n = (w_1 V_n^2/2g)$ gives the dimensionless friction energy rate loss φ_f:

$$\varphi_f = \frac{E_f}{E_n} = \frac{E_p + E_s + E_t + E_d}{E_n} = \varphi_p + \varphi_s + \varphi_t + \varphi_d$$

where

$$\varphi_p = K_p \tag{20}$$

$$\varphi_s = \frac{K_s R^2 M^3}{(1 - R)^2} \tag{21}$$

$$\varphi_t = K_t R^2 (1 + M)^3 \tag{22}$$

and

$$\varphi_d = K_d R^2 (1 + M)^3 \tag{23}$$

$$\varphi_f = K_p + \frac{K_s R^2 M^3}{(1 - R)^2} + K_t R^2 (1 + M)^3 + K_d R^2 (1 + M)^3$$

$$\varphi_f = K_p + \frac{K_s R^2 M^3}{(1 - R)^2} + (K_t + K_d) R^2 (1 + M)^3 \tag{24}$$

The total dimensionless loss factor is

$$\varphi_l = \varphi_f + \varphi_m$$

or

$$\varphi_l = 1 + K_p + (1 + K_t + K_d) R^2 (1 + M)^3 - 2R(1 + M) + (1 + K_s) \frac{M^3 R^2}{(1 - R)^2} - \frac{2M^2 R^2 (1 + M)}{(1 - R)} \tag{25}$$

Dimensionless Static Pressure Rise in the Throat

The expression for dimensionless pressure coefficient at the throat inlet may be subtracted from the value at the throat exit. The result is a dimensionless pressure rise coefficient for the jet pump throat. The pressure coefficient is defined by

$$C_p = \frac{p_x - p_2}{\frac{\gamma V_n^2}{2g}} \tag{26}$$

The value of C_p at the throat inlet

$$C_{p,3} = \frac{p_3 - p_2}{\frac{\gamma V_n^2}{2g}}$$

subtracted from C_p at the throat exit

$$C_{p,4} = \frac{p_4 - p_2}{\frac{\gamma V_n^2}{2g}}$$

yields

$$\Delta C_{p,t} = C_{p_4} - C_{p_3} = \frac{p_4 - p_3}{\frac{\gamma V_n^2}{2g}} \tag{27}$$

Using the momentum equation (eq. (15))

$$p_4 - p_3 = \frac{w_1 V_n}{g_c A_t} + \frac{w_2 V_3}{g_c A_t} - \frac{w_t V_4}{g_c A_t} - \frac{F_{f,t}}{A_t}$$

gives

$$\Delta C_{p,t} = \frac{1}{\frac{\rho V_n^2}{2g_c}} \left(\frac{w_1 V_n}{g_c A_t} + \frac{w_2 V_3}{g_c A_t} - \frac{w_t V_4}{g_c A_t} - \frac{F_{f,t}}{A_t} \right)$$

which becomes

$$\Delta C_{p,t} = 2R + \frac{2R^2 M^2}{1 - R} - (2 + K_t) R^2 (1 + M)^2 \tag{28}$$

MODIFIED ANALYSIS - PERFORMANCE PARAMETERS

The modified analysis is identical to the conventional analysis through equation (8). However, in the modified analysis the development of the mixing velocity profile in the throat is taken into consideration.

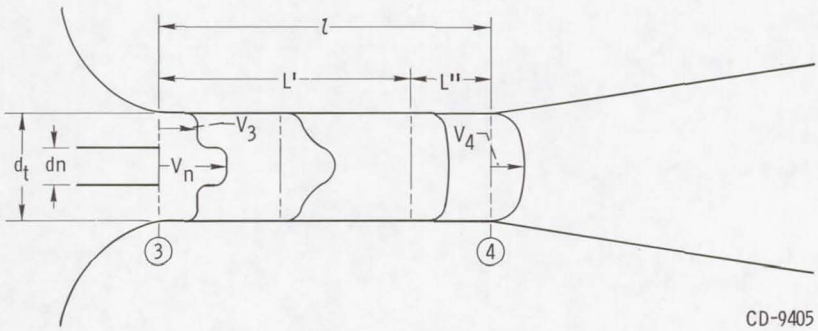

Figure 21. - Schematic representation of mixing profile development.

Figure 21 represents one possible profile development. Only in the length L'' can the flow be considered fully developed pipe flow. Estimation of friction loss in this section only will follow the same procedure as in the conventional analysis.

For the section of length L', it is assumed that the velocity head of the secondary flow increases linearly:

$$\frac{V^2}{2g} = \frac{1}{2}\left(\frac{V_3^2}{2g} + \frac{V_4^2}{2g}\right)$$

Then,

$$h'_{f,t} = f\,\frac{L'}{d_t}\,\frac{V^2}{2g}$$

$$= f\,\frac{L'}{d_t}\,\frac{1}{2}\left(\frac{V_3^2}{2g} + \frac{V_4^2}{2g}\right)$$

$$= K'_t\,\frac{V_n^2}{2g}\left[\left(\frac{V_3}{V_n}\right)^2 + \left(\frac{V_4}{V_n}\right)^2\right]$$

where

$$K'_t = \frac{1}{2}\,f\,\frac{L'}{d_t}$$

The final result, in terms of jet pump dimensionless parameters, is

$$h'_{f,t} = K'_t \frac{V_n^2}{2g}\left[\frac{M^2R^2}{(1-R)^2} + R^2(1+M)^2\right] \tag{29}$$

The total friction loss in the throat is

$$\frac{h_{f,t}}{\frac{V_n^2}{2g}} = \frac{h'_{f,t} + h''_{f,t}}{\frac{V_n^2}{2g}} = (K'_t + K''_t)R^2(1+M)^2 + K'_t \frac{R^2M^2}{(1-R)^2} \tag{30}$$

and

$$p_4 - p_3 = \frac{\gamma V_n^2}{2g}\left[2R + \frac{2M^2R^2}{1-R} - 2R^2(1+M)^2 - K'_t \frac{R^2M^2}{(1-R)^2} - (K'_t + K''_t)R^2(1+M)^2\right] \tag{31}$$

Then, the numerator of the expression for N becomes

$$P_5 - P_2 = \frac{\gamma V_n^2}{2g}\left[2R + \frac{2R^2M^2}{1-R} - (1 + K'_t + K''_t + K_d)R^2(1+M)^2 - (1 + K_s + K'_t)\frac{R^2M^2}{(1-R)^2}\right] \tag{32}$$

and the denominator becomes

$$P_1 - P_5 = \frac{\gamma V_n^2}{2g}\left[1 + K_p - 2R - \frac{2R^2M^2}{1-R} + R^2(1+M)^2(1 + K'_t + K''_t + K_d) + K'_t \frac{R^2M^2}{(1-R)^2}\right] \tag{33}$$

Therefore,

$$N = \frac{2R + \frac{2R^2M^2}{1 - R} - R^2(1 + M)^2\left(1 + K_t' + K_t'' + K_d\right) - \frac{R^2M^2}{(1 - R)^2}\left(1 + K_s + K_t'\right)}{1 + K_p - 2R - \frac{2R^2M^2}{1 - R} + R^2(1 + M)^2\left(1 + K_t' + K_t'' + K_d\right) + K_t'\frac{R^2M^2}{(1 - R)^2}} \tag{34}$$

and

$$\eta = \frac{2RM + \frac{2R^2M^3}{1 - R} - MR^2(1 + M)^2\left(1 + K_t' + K_t'' + K_d\right) - \frac{R^2M^3}{(1 - R)^2}\left(1 + K_s + K_t'\right)}{1 + K_p - 2R - \frac{2R^2M^2}{1 - R} + R^2(1 + M)^2\left(1 + K_t' + K_t'' + K_d\right) + K_t'\frac{R^2M^2}{(1 - R)^2}} \tag{35}$$

DETERMINATION OF FRICTION LOSS COEFFICIENTS

The friction loss coefficients used in the theoretical calculations were determined by component calibrations. It should be clearly understood that they are not therefore dependent on the overall experimental results. The method of determination was direct measurement of pressure differences across each component over a wide range of flow conditions, and, in the case of K_p and K_d, at a retracted nozzle position. This is quite different from measuring efficiency at a fully inserted nozzle position, and calculating values of friction loss coefficient from the theoretical expression for efficiency. The latter method would constitute dependence on overall experimental results, and the theory would obviously check with experiment. The former method, however implies no such guarantee.

The friction loss coefficients could also have been determined by direct estimation, or approximated on the basis of values in the literature (refs. 6 to 8). Component calibration was employed because, when feasible, it provides the most accurate values of friction loss coefficients for the specific components to be used.

The nozzle friction loss coefficient K_p is

$$K_p = \frac{P_1 - p_n}{\frac{\gamma V_n^2}{2g}} - 1 \tag{36}$$

The values for K_p were calculated from jet pump operating runs for which the nozzle was fully retracted into the secondary plenum ($s/d_t = 3.04$). This allowed direct measurement of both inlet and outlet pressure, p_1 and p_n, because p_n corresponds to p_2 when the nozzle exit is retracted into the secondary plenum chamber. The velocity V_n was calculated from primary flow rate Q_1 and nozzle exit area A_n.

For the nozzle corresponding to $R = 0.066$, the average experimentally determined K_p was 0.008; for the $R = 0.197$ nozzle, average measured K_p was 0.036.

When the primary nozzle is fully inserted, station n = station 3 and the secondary inlet friction loss coefficient K_s is

$$K_s = \frac{P_2 - p_3}{\frac{\gamma V_3^2}{2g}} - 1 \tag{37}$$

Experimental values for K_s were calculated from independent calibration test runs in the blowdown mode of operation. The pressures P_2 and p_3 were measured directly, and V_3 was calculated from secondary flow rate Q_2 and from secondary flow area at the inlet to the throat A_3. Also, $K_s = 0.09$ for $R = 0.066$ and $K_s = 0.14$ for $R = 0.197$.

The throat friction loss coefficient K_t for the conventional analysis is

$$K_t = f \frac{l}{d_t} \tag{38}$$

In this analysis, fully developed turbulent pipe flow is assumed to occur for the entire length of the throat. The throat Reynolds number varied from 1.6 to 6.6×10^5. The average value of 4.1×10^5 was used to determine the friction factor ($f = 0.0136$) corresponding to smooth pipes (ref. 19). The average K_t used for a throat length of 7.25 diameters was therefore $K_t = 0.0985$.

For the modified analysis,

$$K_t' = \frac{1}{2} f \frac{L'}{d_t} \tag{39}$$

and

$$K_t'' = f \frac{L''}{d_t}$$

From the total pressure surveys (see figs. 14 to 16), the point at which mixing was completed in the throat was estimated and K_t' and K_t'' were calculated from it. In the case of both area ratios, L'/d_t was determined to be 7.25 and $L''/d_t = 0$. As a result, $K_t' = 0.049$ and $K_t'' = 0$ for both area ratios.

The values for the diffuser friction loss coefficient K_d at both area ratios were calculated from jet pump operating runs with the nozzle in a fully retracted position. The inlet velocity profile to the diffuser was generally uniform when the nozzle was in this position. Values for K_d were calculated from experimentally determined diffuser efficiency values. The derivation of K_d from η_d is as follows:

$$\eta_d = \frac{p_5 - p_4}{\frac{\gamma V_4^2}{2g}\left[1 - \left(\frac{A_4}{A_5}\right)^2\right]} \tag{40}$$

$$\eta_d = 1 - \frac{h_{f,d}}{\frac{V_4^2}{2g}\left[1 - \left(\frac{A_4}{A_5}\right)^2\right]} \tag{41}$$

But,

$$P_4 - P_5 = K_d \frac{\gamma V_4^2}{2g}$$

or

$$K_d = \frac{P_4 - P_5}{\frac{\gamma V_4^2}{2g}} = \frac{h_{f,d}}{\frac{V_4^2}{2g}}$$

Thus,

$$\eta_d = 1 - \frac{K_d}{1 - \left(\frac{A_4}{A_5}\right)^2} \tag{42}$$

or

$$K_d = \left(1 - \eta_d\right)\left[1 - \left(\frac{A_4}{A_5}\right)^2\right] \tag{43}$$

For $\frac{d_4}{d_5} = \frac{1.35}{3.75}$,

$$K_d = 0.983\left(1 - \eta_d\right)$$

The average experimentally determined diffuser efficiency obtained with the nozzle in the fully retracted position was 89.6 percent. The value for K_d corresponding to this efficiency is $K_d = 0.102$.

REFERENCES

1. Sanders, Newell D.; Barrett, Charles A.; Bernatowicz, Daniel T.; Moffitt, Thomas P.; Potter, Andrew E., Jr.; and Schwartz, Harvey J.: Power for Spacecraft. Proceedings of the NASA-University Conference on the Science and Technology of Space Exploration. Vol. 2. NASA SP-11, Vol. 2, 1962, pp. 125-150.

2. Chalpin, E. S.; Pope, J. R.; and Foss, C. L.: Development of a SNAP-8 Pump for Mercury Service. AIAA Specialists Conference on Rankine Space Power Systems. Vol. I. AEC Rep. No. CONF-651026, Vol. 1, 1965, pp. 171-185.

3. Lewis, R.: Jet Inducer Experimental Analysis Using Multiple Nozzles in Mercury and Water. Rep. No. ER-6420, TRW, Inc., May 2, 1966.

4. Lewis, R. A.: Jet Inducer Design Study for High Performance Mercury Pumps. Rep. No. ER-6758, TRW, Inc., Feb. 9, 1966.

5. Rankine, J. M.: On the Mathematical Theory of Combined Streams. Proc. Roy. Soc. (London), vol. 19, 1870, p. 90. (Referenced in Mueller, N.H.G.: Water Jet Pump. Proc. ASCE, vol. 90, no. HY3, pt. 1, May 1964, pp. 83-112.)

6. Gosline, James E.; and O'Brien, Morrough P.: The Water Jet Pump. Univ. California, Publ. in Eng., vol. 3, no. 3, 1934, pp. 167-190.

7. Cunningham, Richard G.: The Jet Pump as a Lubrication Oil Scavenge Pump for Aircraft Engines. (WADC TR-55-143), Pennsylvania University, July 1954.

8. Mueller, N.H.G.: Water Jet Pump. Proc. ASCE, vol. 90, no. HY3, pt. 1, May 1964, pp. 83-112.

9. Citrini, Duilio: A Contribution to Jet-Pump Design. LaHouille Blanche, Grenoble, France, vol. 11, no. 6, Dec. 1956, pp. 837-842.

10. Curtet, Roger: Jet Flow Between Walls. Detailed Study of Ejector Pumps. Rep. No. RSIC-461, Redstone Scientific Information Center, Army Missile Command, Sept. 1965. (Available from DDC as AD-473568L.)

11. Curtet, R.; and Ricou, F. P.: On the Tendency to Self-Preservation in Axisymmetric Ducted Jets. J. Basic Eng., vol. 86, no. 4, Dec. 1964, pp. 765-776.

12. Barchilon, M.; and Curtet, R.: Some Details of the Structure of an Axisymmetric Confined Jet with Backflow. J. Basic Eng., vol. 86, no. 4, Dec. 1964, pp. 777-787.

13. Vogel, R.: Theoretical and Experimental Investigation of Air Ejectors. Maschinenbautechnik, vol. 5, 1956, pp. 619-637.

14. Hansen, Arthur G.; and Kinnavy, Roger: The Design of Water-Jet Pumps. I - Experimental Determination of Optimum Design Parameters. Paper No. 65-WA/FE-31, ASME, Nov. 1965.

15. Schulz, F.; and Fasol, K. H.: Wasserstrahlpumpen zur Forderung von Flussigkeiten. Springer Verlag (Vienna), 1958.

16. Kroll, A. Edgar: The Design of Jet Pumps. Chem. Eng. Progr., vol. 1, no. 2, Feb. 1947, pp. 21-24.

17. Pai, Shih-i: Fluid Dynamics of Jets. D. Van Nostrand Co., Inc., 1954.

18. Rayle, R. E.: Influence of Orifice Geometry on Static Pressure Measurements. Paper No. 59-A-234, ASME, 1959.

19. Moody, Lewis F.: Friction Factors for Pipe Flow. Trans. ASME, vol. 66, no. 8, Nov. 1944, pp. 671-684.

NASA-Langley, 1968 —— 15 E-3899